UNIVERSITY OF TWENTE.

Faculty of Electrical Engineering, Mathematics & Computer Science

Characterization of Vibrating Intrinsic Reverberation Chamber and Comparison with Classical Reverberation Chamber for Antenna Efficiency Measurements

Rufat Alizada

M.Sc. Thesis
December 2018

Supervisors:
dr. A. Alayón Glazunov
prof. dr. ir. ing. F.B.J. Leferink
dr. ir. A.B.J. Kokkeler
I.Bilal, MSc

Telecommunication Engineering Group
Faculty of Electrical Engineering,
Mathematics and Computer Science
University of Twente
P.O. Box 217
7500 AE Enschede
The Netherlands

Summary

The rapid expansion of wireless communication industry calls for cost- and time-efficient electromagnetic (EM) measurements. Among the most important we have the characterization of antennas, or wireless devices in general, and the electromagnetic compatibility (EMC) testing of various electronic equipment. Over the past two decades, Reverberation Chambers (RC) have established themselves as an useful and accurate testing and characterization tool for measurements of a wide range of devices and figures of merit with applications in the wireless communications industry, e.g., smartphones, access points, and small and medium base stations. An RC is a statistical measurement facility consisting of a large metallic hollow cavity sustaining a large number of resonating electromagnetic modes, i.e., a resonating cavity. Irregularly shaped moving paddle stirrers are employed for mixing electromagnetic fields in order to obtain many statistically independent samples. Such facilities are ideally suited for performing radiated power measurements of either an antenna or a device under test (DUT), especially to determine the radiation efficiency of antennas. There have been several reverberation chamber techniques proposed over the years for measuring the antenna efficiency requiring the chamber to be spatially uniform, i.e., isotropic on average, with a large number of modes and high mode density. However, to make the RC well-stirred (i.e., with a uniform field distribution on average), a large number of independent samples (stirrer positions) are required. Consequently, the measurements can become long depending on the electrical size of the DUT in relation to the RC's testing volume and also the figure of merit of interest. Moreover, if a physically large RC is employed, it may restrict its use due to the increased weight of the larger metallic cavity.

Therefore, the primary focus of this thesis is to evaluate the use of the vibrating intrinsic reverberation chamber (VIRC) as a lightweight and fast alternative to antenna efficiency measurements. The VIRC is a transportable reverberation chamber with varying angles between wall, floor, and ceiling, where wave diffusion is achieved by the vibration of the flexible walls. Presented is a further study into the VIRC and various measurement procedures associated with it. For the purpose of showing whether the VIRC may have an impact on the implementation of antenna efficiency measurements, we have carried out a comparison of measurements of two wideband antennas, namely,

vertically polarized, discone antenna and a double ridge guide (DRG) horn antenna. Measurements were performed in a classical RC (1.5 m x 1.3 m x 1 m) and a VIRC (1.5 m x 1.2 m x 1 m) at the University of Twente, Enschede, the Netherlands. In comparison, we consider the following characteristics of the two RCs: their Q-factors and the enhanced backscatter coefficients. The antenna efficiency is measured using two subcategories of the non-reference antenna measurement method, namely, the one-antenna and the two-antenna methods.

The findings of this thesis are the following. First, it is observed that the effect of non-ideal field uniformity in both RCs, as defined by the enhanced backscatter coefficients being different from 2, is eliminated by the two-antenna method. Second, in spite of the two chambers differing in dimensions and stirring mechanisms, the antenna efficiency measured using the two-antenna method is similar in both the classical RC and the VIRC. VIRC has very close agreement between the results calculated by using both one- and two-antenna methods for frequencies above 700 MHz (with combined relative uncertainty of 0.12 for AUT1 and 0.08 for AUT2) but Classical RC's one-antenna and two antenna methods provide relatively larger difference in the efficiencies ($<$5% for AUT2 and 12% for AUT1). These results demonstrate the feasibility of implementing non-reference antenna efficiency measurements in VIRC and its use as an alternative tool for antenna efficiency measurements. The presented results add to the wealth of other results aiming at the VIRC, and RC in general, becoming a fully standardized and accepted facility within the wireless and EMC measurement industries.

Acknowledgement

This thesis represents final work of master program in Telecommunication Engineering (TE), track of Master of Science in Electrical Engineering at the Faculty of Electrical Engineering, Mathematics and Computer Science of University of Twente in Enschede, the Netherlands.

Firstly, I would like to thank my supervisor dr. A. Alayón Glazunov for giving me the opportunity to pursue my studies at the University of Twente and to work on this project. Thanks to his guidance and his patience I achieve to complete my research. Special thanks are addressed to my thesis advisor dr.ir. R.A. Vogt-Ardatjew who has always been willing to help me with any difficulties in my research.

Moreover I wish to thank all the members of the TE group and BOZ in the department of EEMCS. Special thanks are addressed to E.M. Hannink, S.Padberg-Heskamp and H.Masselink.

My sincerest thanks go out to all my friends that I met in Enschede and made it feel like home. Thank you for all the conversations, the dinners, time that we spent together and for all your help and advice during my master. All you have contributed to make a very pleasant environment.

Finally I would like to thank my family for believing in me, encouraging and support me in many ways in all my life.

Rufat Alizada, Enschede 2018

Contents

List of acronyms

AC anechoic chamber

AUT antenna under test

BER bit error rate

CDF cumulative distribution function

CI confidence interval

CLT central limit theorem

CW continuous wave

DRG double ridge guide

DUT device under test

EM electromagnetic

EMC electromagnetic compatibility

EMI electromagnetic interference

FD frequency domain

FDTD finite-difference time-domain

FS frequency stirring

GPIB general purpose interface bus

i.i.d independent and identically distributed

IEC international electrotechnical commission

IFFT inverse fast Fourier transform

IoT Internet of Things

LUF lowest usable frequency

MIMO multiple-input multiple-output

OTA over-the-air

PDF power delay profile

Q-factor quality factor

RBW resolution bandwidth

RC reverberation chamber

RF radio frequency

STD standard deviation

TD time domain

USRP universal software radio peripheral

VIRC vibrating intrinsic reverberation chamber

VNA vector network analyzer

Chapter 1

Introduction

1.1 Motivation

Wireless communication is today one of the most exciting and rapidly growing areas within the information technologies. New technologies such as 5G and the Internet of Things (IoT) promise new capabilities and use cases, which are set to impact not only consumer services but also many industries embarking on their digital transformations. In order to deliver pervasive coverage, 5G wireless systems will operate within two main frequency ranges: sub-6 GHz and above 6 GHz. Over-The-Air (OTA) characterization of wireless devices, e.g., mobile phones, laptops, access points, and base stations, is critical to the successful deployment of 5G. OTA measurements require the use of well-characterized reference antennas. Given the above 5G frequency ranges it is essential that antennas are capable of operating with satisfactory radiation efficiency and maintain good radiating performance over a wide operating bandwidth. This exerts a pressure to develop cost- and time-efficient techniques for efficiency characterization of antennas while providing good enough accuracy.

Over the past decade, Reverberation Chambers (RC) have been used more and more as a promising tool for the measurement of antenna characteristics for wireless communications applications. A typical RC is, at its most fundamental level, an electrically large metallic box featuring one or more metallic stirrer(s) to create changing boundary conditions in order to obtain statistically uniform electromagnetic (EM) field. The principle of operation of the RC is based on the existence of multimode resonance mixing [1], which can be achieved either by mode-tuned or mode-stirred methods. The movement of objects inside the chamber is referred to as mode-stirring. Mode-tuning, on the other hand, is a technique of moving the stirrer in discrete steps and performing the measurement while it is stopped. When an antenna is placed in the chamber it will excite a large number of EM modes that have resonances near the frequency of excitation. The rotating paddle stirrer (from now on just stirrer) creates an environment in the RC with statistically independent samples of the field. Such an RC is ideally

suited for performing radiated power measurements of an antenna under test (AUT), and as such, it is possible to determine its radiation efficiency.

There are mainly two kinds of RCs, defined by their various stirring strategies. One of such is the Vibrating Intrinsic Reverberation Chamber (VIRC). The VIRC is a chamber that consists of conductive cloth that forms the flexible walls (including the floor and ceiling) and uses mechanic vibration of the walls as the means to create a statistically uniform (i.e., isotropic on average) and random polarized field at much lower frequencies than conventional RCs [2], [3]. Numerical simulation based on the FDTD (finite-difference time-domain) algorithm has been done in [4], and it shows very good field uniformity and isotropic electromagnetic field. Nowadays, the VIRC is being used in many applications such as shielding effectiveness [5] and in-situ EMC testing [2], [6]. Because of the large number of independent samples in a VIRC, it also allows a better prediction of extreme field strengths as compared to mode-tuned chambers. Hence, VIRC can be used to better estimate the risk of electromagnetic interference (EMI) in semi-enclosed environments [7], [8]. Also, the larger dynamic change can result in more accurate communications tests involving BER (Bit Error Rate) and throughput measurements in multipath environments [9].

1.2 Scope and Objectives

In this thesis, we characterize and evaluate the performance of VIRC for antenna efficiency measurements. For the purpose of whether different reverberation chambers may impact on the implementation of these measurements, we have carried out a comparison on wideband antennas measurements in a classical RC and in a VIRC at the University of Twente, Enschede, the Netherlands. The characteristics of the two RCs such as Q-factors, decay constants, and enhanced backscatter coefficients are analyzed. Also, the measured antenna efficiency is compared using the measurements in two subcategories of the non-reference antenna method namely the one-antenna and the two-antenna methods [10]. The goal of this study is to better understand the VIRC, help develop guidelines for antenna efficiency measurements performed in it and evaluate VIRC as an alternative testing facility for antenna efficiency measurements. The main research question answered in this report is: “How does the VIRC impact the antenna efficiency measurements over the operation bandwidth of the antennas?"

1.3 Report Organization

The report is divided into six chapters. The theoretical background and current techniques for characterizing the RCs are presented in Chapter 2. Chapter 3 goes into detail about antenna efficiency measurement methods and uncertainty associated with

it. In Chapter 4, the measurement campaign that is used to experimentally study the effect of RCs on the antenna efficiency measurements is explained. Chapter 5 presents the analysis of the RC characterization measurements and the measured antenna efficiency in both chambers and any difference therein. Finally, in Chapter 6, conclusions are drawn and recommendations for future work are made.

Chapter 2

RC Characterization

The sub-field of electromagnetics concerned with the physical foundations of reverberation chamber cavity theory is a well-studied research topic. We owe much to scientists and educators such as Harrington [11], Balanis [12], Kraus [13] and more recently Hill [14] for their pioneering work in this area. In [14], Hill showed that for electrically large, complex cavities, with spatially- and time-varying field distributions the details of the cavity geometry and loading objects are not expected to be precisely known [14]. In such cases, the deterministic mode theory is not appropriate for predicting the field distribution properties while the statistical theory becomes useful [11] - [14].

This chapter reviews a few fundamental concepts concerning the reverberation chambers (RC). First, the electromagnetic environment of reverberation chamber is briefly revisited together with the concept of spatial uniformity and methods to characterize it. Different methods used to characterize the spatial uniformity of the RC can be found in [15]. Second, the Q-factor of the chamber and the two commonly used approaches to measure it are discussed.

2.1 Spatial Uniformity

In a well-calibrated RC chamber with good measurement equipment, the dominant source of error is the spatial dependence of the fields [14]. To ensure a low uncertainty in the antenna characterization measurements, it is important to have a spatially uniform field distribution throughout the chamber, i.e., the energy density in the chamber should be as uniform as possible. This will ensure that the measurement results are, on average, independent of the exact measurement location within the working volume of the RC.

2.1.1 Electromagnetic Field Distribution

A fundamental mathematical principle applied to many statistical models is the central limit theorem (CLT). It implies that a sum of many independent and identically distributed (i.i.d.) random variables tends to become Gaussian (or normal) distributed [14].

In RCs the field measured at a certain point within its volume is the result of the superposition of several waves or modes. The real and imaginary parts of the electric field are both Gaussian distributed with zero mean in a well-stirred reverberation chamber if enough independent waves (i.e., modes) are excited within the chamber. In this case, the magnitude of the electric field becomes Rayleigh distributed when measured over time and at various points within the RC volume. The Rayleigh distribution is a special case of the Rician distribution when independent modes are generated with the moving stirrers in the chamber [14], [16], [17]. This is valid for an ideal world, but in reality, unstirred field components might be present, i.e., a component associated with the energy coupling between the transmitter and the receiver without any additional interaction with the stirrer.

The Rician probability density function (PDF) for the electric field in the RC is given by

$$f(|E_x|) = \frac{|E_x|}{\sigma^2} I_0\left(\frac{|E_x||E_{dx}|}{\sigma^2}\right) e^{-\frac{|E_x|^2+|E_{dx}|^2}{2\sigma^2}} \tag{2.1}$$

where I_0 is the modified Bessel function of the zero-th order, $|E_x|$ is the amplitude of the complex electric field from the modes that interact with changing environment of RC, $|E_{dx}|$ is the amplitude of the complex unstirred field component and σ^2 is the variance of the magnitude of the real or imaginary parts of the stirred electric field.

A Rician distribution is characterized by the Rician K-factor, which is defined as the ratio of the signal power in the unstirred components over the stirred power. For K=0 equation (2.1) reduces to Rayleigh distribution. Typically in reverberation chambers the K-factor is very low, but not zero. The K-factor is an important parameter to define the electromagnetic environment in a reverberation chamber.

A straightforward method to characterize the spatial uniformity is by graphical inspection/comparison, i.e., the PDF of the measured data and the theoretical Rayleigh PDF (see (2.1) with $|E_{dx}| = 0$) are plotted on the same graph. While this technique is relatively easy to carry out, one must be careful when interpreting the results. The measured PDF of an antenna placed in a single position may well approximately look like the theoretical PDF. However, it will still be necessary to take these measurements in multiple locations within the chamber and compare the PDFs for each position. In doing so, we need to ensure that they are not only of the correct type, but that there is little variation in their respective magnitudes and shapes relative to each other. Hence, in this way, we may establish uniformity over time and also within the test volume of

the RC.

2.1.2 Enhanced backscatter Coefficient

A more accurate method to characterize the field distribution uniformity consists in estimating the variance of the measured data [17] as a function of antenna position in the RC. This technique is carried out by placing antennas at many positions within the RC and taking measurements for each antenna position. The standard deviation of the measured field amplitudes gives a measure of the spatial uniformity of the chamber. While these measurements have the potential of giving a very good characterization of the RC's spatial uniformity, they can also be difficult or impractical to perform. Therefore, the method used in this thesis is the evaluation of a spatial uniformity using the measurements of the enhanced backscatter coefficient (e_b), as described in [15].

In EM, the term backscatter refers to the scattering of an EM wave towards the direction of the source. Enhanced backscatter refers to the phenomenon by which the sum of the scattered fields in the backscatter direction is larger in magnitude than the scattered fields in other directions. The factor of backscatter enhancement, termed the enhanced backscatter coefficient, is equal to the ratio of the average power at the source to the average power in other locations within the scattering space. The enhanced backscatter coefficient e_b is defined mathematically as

$$e_b = \frac{\langle P_{rf} \rangle}{\langle P_{Rx} \rangle} \tag{2.2}$$

where the symbol $\langle\rangle$ represents an ensemble average, P_{Rx} is the power at a receive antenna inside the chamber and P_{rf} a portion of the energy that reflects off the chamber walls and stirrer towards the transmit antenna.

The value of the e_b depends on the RC's spatial uniformity. In an RC measurement with well-mixed field modes, the e_b has been observed to take on values that are close to 2 [14]. Deviations from this value are an indication that there is spatial dependence of the fields within the RC. In addition, [15] observed the changes in the measured e_b over frequency and used it to directly estimate the error associated with spatial dependence in the measured data. The derivation of the e_b and the estimation of the uncertainty will be discussed in the following sections.

2.2 Quality Factor

The quality factor Q is defined as the ability of the resonating chamber to store electromagnetic energy and to reverberate. It is an important performance parameter of an RC because it determines the field enhancement and the decay time [17]. The Q-factor

is defined as

$$Q = \frac{\omega U}{P_d} \tag{2.3}$$

where U is the energy stored in the chamber, P_d is the power dissipated in the chamber, and $\omega = 2\pi f$ is the angular frequency measured in radians per seconds and f is frequency measured in Hertz.

A significant information that the quality factor provides is that by knowing the Q-factor of an RC and therefore the losses in it, it is possible to predict the amount of energy needed to produce the required field strength. A high Q-factor means that the cavity has low losses and less energy is required to produce a given field strength level as compared with a cavity with lower quality factor and higher losses. Moreover, the Q-factor is related to the mode excitation [14], [18].

It is possible to measure the Q-factor using two commonly used measurement approaches, e.g., frequency domain and time domain measurements [19], [20]. According to [21], depending on the used chamber size and antennas, there is a systematic offset when comparing Q_{TD} and Q_{FD}. The estimates of Q_{TD} are higher than those obtained from frequency-domain. In [14], Hill suggests that the Q_{TD} obtained from the decay time measurements are less affected by antenna efficiency and impedance mismatch than the Q_{FD}; hence, the discrepancy. Recently, Holloway et al. [10] have introduced simple antenna efficiency measurement methods using RC based on the fact that the difference in the Q-factor can be attributed to the radiation efficiency of the antennas used in the measurement. This technique is used in this thesis in order to measure and compare the antenna efficiency measured in both RCs. The methods are described in the following section.

2.2.1 Frequency Domain Measurements

In the frequency domain, the Q_{FD} measurement techniques are commonly referred to as CW (Continuous Wave) measurements. The Q-factor can be obtained using [10]

$$Q_{FD} = \frac{16\pi^2 V}{\lambda^3} \langle |S_{21}|^2 \rangle \tag{2.4}$$

where V is the chamber volume, λ is the wavelength and $\langle |S_{21}|^2 \rangle$ is the ensemble average of the transmission coefficients between two antennas obtained from different independent samples, where these samples are obtained by different antenna efficiency (stirring) positions, averaging of a "small" band of frequencies, and/or measuring the power at different locations in the chamber.

2.2.2 Time Domain Measurements

In the time domain, Q_{TD} measurement techniques are referred to as power decay profile measurements. The quality factor is given by

$$Q_{TD} = \omega \tau_{RC} \tag{2.5}$$

where τ_{RC} is the chamber time constant. Details for determining τ_{RC} are found in [18] and [22]. In order to determine τ_{RC} one should first obtain the power delay profile (PDP) of the chamber

$$PDP(t) = \langle |h(t,n|^2 \rangle \tag{2.6}$$

where the ensemble average is taken over the stirrer position n, and $h(t,n)$ is the impulse response of the chamber for the nth stirrer position. In this expression, the $h(t,n)$ is given by computing the Inverse Fast Fourier Transform (IFFT) over a certain frequency range

$$h(t,n) = IFFT[S_{21_n}(f)] \tag{2.7}$$

Once the $PDP(t)$ is obtained, τ_{RC} can be determined by neglecting the early time behavior of the RC by

$$PDP(t) = \langle |h(t,n|^2 \rangle = P_0 \mathrm{e}^{-t/\tau_{RC}} \tag{2.8}$$

where $\mathrm{e}^{(.)}$ is the exponential function.

This method, however, is not suitable for the VIRC, since the implementation of this method requires the steadiness of the environment for the duration of the frequency sweep. Therefore, in this thesis, the method of measuring the Q-factor directly in time domain [23] has been adopted to measure and compare the average composite Q-factor of both chambers. In this method, the Q_{TD} is found by radiating a short pulse into the chamber from one antenna and examining the exponential decay rate of the received mean reverberant signal, averaged over numerous stirred field samples [20]. In [23], it is shown that Q-factor can be extracted directly from linear averaged traces of received power using (2.5) and average logarithmic decrement of the free-decay field of energy density stored in any point of the enclosure [24]

$$Q_{TD} = \frac{20\pi f \Delta t}{\ln(10)\Delta P_{r|dB}} = \frac{20\pi f \Delta t}{\ln(10)\Delta E_{dB}} \tag{2.9}$$

where f is the frequency, $\ln(.)$ is the logarithmic function in the natural base, P_r the received power at the antenna port ($\Delta P_{r|dB}$ means the dB reading of ΔP_r) and ΔE_{dB} is the reading of free-decay field of energy density stored in any point of the enclosure in dB.

This method requires an appropriately fast equipment (RF pulse generator and detector) but is usable in any conditions, including a continuously shaking VIRC, where the measurement is much faster than the rate of change of the field [7].

Chapter 3

Antenna Characterization

3.1 Antenna Efficiency

The antenna radiation efficiency (η) is a classical antenna performance parameter that has shown to be very convenient in characterizing antennas for mobile and wireless terminals that operate in complex multipath environments. Normally η is expressed in percentage although it is also common to express it in dB. A good and efficient antenna should have very high efficiency, ideally 100% (i.e., 0 dB). It should be pointed out that η is determined by the antenna loss but does not include the antenna impedance mismatch. The mismatch between the feedline/connector and the antenna is taken into account by the total efficiency (η_T) which is defined as the ratio of the power radiated (P_r) to the power available at the antenna port (P_s) and can be expressed as

$$\eta_T = \frac{P_r}{P_s} = (1 - |\Gamma|^2) \cdot \eta \tag{3.1}$$

where Γ is the reflection coefficient (the same as the S-parameter S_{11} or S_{22}) which is complex number and can be easily obtained using a VNA (vector network analyzer). In this thesis, we are concerned with determining both the total efficiency (ration of the power radiated to the power available at the antenna port) and the radiation efficiency (ration of the power radiated to the power accepted by the antenna port).

3.2 Non-Reference Antenna Efficiency Measurements

Starting almost two decades ago, reverberation chambers (RCs) have been employed for measuring antenna efficiency due to their simplicity and easy setup implementation [25]–[29]. The use of RCs to measure radiation efficiency was introduced by Rosengren et al. [30]. Since then, several measurement techniques in the area of efficiency measurements have been evaluated, e.g., [27]–[29], [31]. Lately, cost-efficient methods showing how universal software radio peripheral (USRP) can be used to measure the

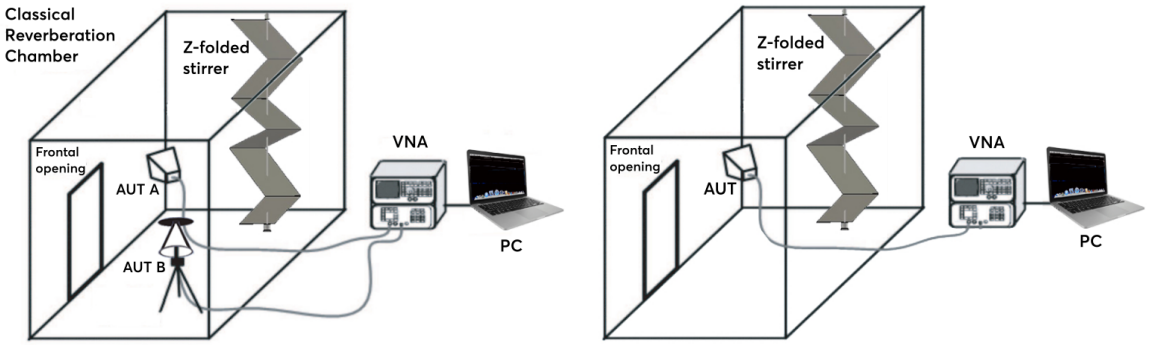

(a) Two-antenna measurement method. *(b)* One-antenna measurement method.

Figure 3.1: RC setup for non-reference measurement methods for determining the antenna efficiency.

complete passive over-the-air (OTA) performance of multiport antennas for multiple-input multiple-output (MIMO) systems in RC has been shown in [32]. Furthermore, it has been shown that RCs can be used to measure the OTA throughput of active devices, such as wireless modems and mobile phones through indirect assessment of antenna efficiency if the device has an accessible antenna port [33].

One commonly used antenna efficiency measurement method in RCs (e.g., specified in the IEC standard [34]) was first introduced using either a reference antenna with known efficiency or two identical antennas with the same efficiency. More recently, the techniques for determining the antenna efficiency without the need for a reference antenna or two identical antennas have been introduced, with good measurement results [10]. Not only are the non-reference antenna methods simpler than the reference antenna method, but also uncertainties that the reference antenna may introduce no longer exist. However, there are some restrictions on the RCs and the antennas-under-test (AUT) when applying the non-reference antennas methods.

The non-reference antenna method for measuring antenna efficiency in RCs is briefly described below [10]. The method is based on the fact that the Q-factor of an RC measured in time-domain Q_{TD} is different from the measured in the frequency-domain Q_{FD} [18]. The ratio of FD to TD Q-factors is equal to the product of the total efficiencies of the two antennas is given by

$$\eta_A^{total}\eta_B^{total} = \frac{Q_{FD}}{Q_{TD}} \tag{3.2}$$

where η_A^{total} and η_B^{total} are the total efficiencies of the antennas at ports A and B, respectively.

The process of using an RC for antenna efficiency measurements is relatively straightforward. In addition to the RC, the equipment required is PC and a network analyzer.

In [10] it is shown that S-parameters can be used to derive the AUT efficiency, which for the one-antenna method, the radiation efficiency is given by

$$\eta^{total,1} = \sqrt{\frac{C_{RC}\langle|S_{11,s}|^2\rangle}{2\,\omega\,\tau_{RC}}} \tag{3.3}$$

while in the two-antenna method the efficiency can be computed as follows

$$\begin{aligned} \eta_A^{total,2} &= \sqrt{\frac{C_{RC}\langle|S_{11,s}|^2\rangle}{e_b\,\omega\,\tau_{RC}}} \\ \eta_B^{total,2} &= \sqrt{\frac{C_{RC}\langle|S_{22,s}|^2\rangle}{e_b\,\omega\,\tau_{RC}}} \end{aligned} \tag{3.4}$$

where $\langle|S_{11,s}|^2\rangle$ and $\langle|S_{22,s}|^2\rangle$ are the stirred energy contribution to scattering parameters S_{11} and S_{22}, respectively. C_{RC} is the chamber constant of the reverberation chamber at a certain wavelength λ and given as

$$C_{RC} = \frac{16\pi^2 V}{\lambda^3} \tag{3.5}$$

where τ_{RC} is the decay constant or the decay time of the chamber and V is the chamber volume.

The first superscript "total" in (3.3) and (3.4) is used to emphasize that this is the total efficiency of the AUT, and the second superscript is used to emphasize the number of antennas required in the approach. In the one-antenna method when the same antenna is used as both the transmit antenna and the receive antenna, η_A=η_B. It is also assumed that the reverberation chamber is well "stirred" or that a perfectly statistically uniform electromagnetic field is created inside the RC, therefore the total efficiency of the antenna is derived as shown in (3.3). In the two-antenna method, two antennas are used in the test and the assumption of the well "stirred" environment is no longer needed. It is more realistic to replace 2 in the denominator of (3.3) by the enhanced backscatter coefficient e_b of the reverberation chamber. Thus, the total antenna efficiency for both antennas are derived within a single measurement and the equations are given by (3.4). Figures 3.1a and 3.1b illustrate both setups in classical RC measurements.

Both one- and two-antenna methods require either the measurement of $\langle|S_{11}|^2\rangle$, $\langle|S_{22}|^2\rangle$, and/or $\langle|S_{21}|^2\rangle$. Simple measurement of the scattering parameters with a VNA would have contributions from the stirred energy and unstirred energy inside the chamber. Hence, the chamber insertion loss S_{21} can be expressed as a sum

$$S_{21} = S_{21,s} + S_{21,us} \tag{3.6}$$

where $S_{21,us}$ is the unstirred component and $S_{21,s}$ is the component associated with the stirred energy in the chamber. In [17] and [35], it was described how the stirred energy

can be calculated from the scattering parameters

$$\langle |S_{21,s}|^2 \rangle = \langle |S_{21} - \langle |S_{21} \rangle|^2 \rangle \tag{3.7}$$

with similar expressions for $\langle |S_{11,s}|^2 \rangle$ and $\langle |S_{22,s}|^2 \rangle$. Those parameters, together with the knowledge of the chamber decay time τ_{RC} are used in (3.3) and (3.4) to determine the total efficiency of the AUT.

The radiation efficiency of AUT can be obtained by correcting the measured S-parameters to account for the antenna mismatch. In [36] it is explained how the received power can be corrected for antenna mismatch

$$\langle |S_{21,s}|^2 \rangle_{cor} = \frac{\langle |S_{21,s}|^2 \rangle}{(1 - |\langle S_{11} \rangle|^2)(1 - |\langle S_{22} \rangle|^2)} \tag{3.8}$$

where $|\langle S_{11} \rangle|^2$ and $|\langle S_{22} \rangle|^2$ are the free-space reflection coefficients of the antennas under the test.

Previously mentioned in Section 2.1.2, e_b is defined as the enhanced backscatter coefficient (a quantity analogous for backscatter that has been derived for scattering by a random medium). In [14] and [37], it is shown that in an ideally performing RC (implying that the chamber is well stirred with a large number of modes and a large mode-density), e_b is equal to 2. In [38], e_b was used as a quality measure for the chamber performance. Indeed, the deviation of e_b from 2 represents imperfection in the chamber and can be used as an alternative approach for assessing how well an RC is performing. The enhanced backscatter coefficient is given as

$$e_b = \frac{\sqrt{\langle |S_{11,s}|^2 \rangle \langle |S_{22,s}|^2 \rangle}}{\langle |S_{21,s}|^2 \rangle} \tag{3.9}$$

The expression (3.9) does not depend on the antenna efficiency of the measurement antennas and serves as a figure of merit to characterize the field uniformity in an RC.

3.3 Measurement Uncertainty

Every measured quantity has a measurement uncertainty associated with it. In the following sections the accuracy of the different measurement methods performed in different chambers will be compared. In each method, many samples are the measured quantities are obtained, either over different measurement configurations or over a bandwidth of frequencies. The sample standard deviation of different samples P_n of a quantity P, gives the absolute measurement uncertainty $\widehat{u}_P$ in P (see e.g., [39])

$$\widehat{u}_P = \sqrt{\frac{1}{N-1} \sum_{n=1}^{N} \left[\langle P_n \rangle - \frac{1}{N} \sum_{n=1}^{N} \langle P_n \rangle \right]^2} \tag{3.10}$$

In order to study the relative impact of mode-stirring techniques on measurement uncertainty, we will utilize a normalized form of uncertainty $\widehat{u}_P$. From (3.10), the relative measurement uncertainty $\widehat{\widehat{u}}_P$ is defined as

$$\widehat{\widehat{u}}_P = \frac{\widehat{u}_P}{\frac{1}{N}\sum_{n=1}^{N}\langle P_n \rangle} \tag{3.11}$$

This relative uncertainty facilitates comparisons of the measured results to those that would be expected for an ideal measurement procedure in an ideal reverberation chamber [39]; that is, one with perfect mode stirring (no unstirred energy), no correlation between measurements, and no measurement noise. The uncertainty defined above is not complete since it does not include effects of the noise floor. However, the above uncertainty can be effectively used to compare different computational methods used for characterizing the RC as shown in [15]. Different methods used to characterize the RCs may result in different values of $\widehat{\widehat{u}}_P$. This could be used to derive the confidence interval, an estimate of the error bounds that result from the use of statistical measurements.

Using the concepts presented in Section 3.2 and data collected from both RCs, the steps required in obtaining the total efficiency of the AUT have been shown. According to [15], the uncertainty estimation method obtained from e_b can be used to provide a measure of confidence in the computed total antenna efficiency. In a chamber with a certain Q-factor, it can be shown that the standard deviation of the obtained distribution, e.g. of averages, is proportional to its mean. Therefore, the confidence interval (CI) calculated from the e_b data can be scaled to any other value recorded in the same environment. This method follows the arguments made in [10] that the mean squared terms e_b, $\langle|S_{11,s}|^2\rangle$ and $\langle|S_{11}|^2\rangle$ should have similar relative uncertainty. Thus, the relative uncertainty estimate, $\widehat{\widehat{u}}_{e_b}$, can be used to estimate the uncertainty of the different mean squared terms used in antenna efficiency equations [38]. Spatial uniformity is a fundamental assumption to all RC theoretical analysis, and thus the spatial dependence of the RC is directly related to the uncertainty of the measurements. The other term in (3.4) that can vary with the RC spatial dependence is τ_{RC}. The uncertainty of τ_{RC} can be found using multiple configurations of the aforementioned Q_{TD} and Q_{FD} measurements. The standard uncertainty computed from these different terms can be entered in to (3.4) to give the CI, given by [38]

$$\eta_{CI}^{total,2} = \sqrt{\frac{C_{RC}\cdot(\langle|S_{11,s}|^2\rangle \pm \widehat{\widehat{u}}_{e_b}\langle|S_{11,s}|^2\rangle)}{(e_b \pm \widehat{\widehat{u}}_{e_b}e_b)(Q \pm \widehat{\widehat{u}}_{Q_{TD}}Q)}} \tag{3.12}$$

where the parameters are explained above and given in (2.9), (3.5), (3.7) and (3.10).

Chapter 4

Measurement Setup

This chapter covers the measurement setup used in experimental tests aiming to compare two reverberation chambers and characterize the VIRC. This includes the antenna efficiency setup and experiments carried out to measure Q-factor in both frequency and time domains.

4.1 Antenna efficiency Setup

Figures 4.1 and 4.2 illustrate the actual measurement setups inside the two chambers, i.e., a classical RC and a VIRC, respectively. Classical RC has a single mechanical mode stirrer. It is a chamber with dimensions 1.5m $\times$ 1.3m $\times$ 1m and a 0.6m $\times$ 0.6m frontal opening sealable with a hatch. As it can be seen in Figure 4.1b, inside the chamber there is a typical vertical Z-folded mode stirrer with 0.4m in diameter located in the back. It is rotated using a stepper motor controlled with a computer. Therefore allowing to use both mode-stirring and mode-tuning techniques with very high resolution (0.007° with microstepping).

The VIRC employed in this thesis is similar to the one presented in [2]. Its dimensions are 1.5m $\times$ 1.2m $\times$ 1m, making it only slightly (about 8%) smaller than the used classical RC. The mode-stirring is performed by introducing local changes on the surface of the chamber walls, i.e., changing the boundary conditions, which are made of a flexible, but highly conductive fabric. The mechanical motion is produced by two DC motors, which pull the fabric from two sides. Due to the walls' movement inducing the complex and unpredictable behavior of the flexible material, the VIRC is expected to provide a significantly higher amount of independent positions than the classical RC since each field state in the chamber is sufficiently random [7]. However, because the shaking motion is a continuous process, the VIRC can only operate in mode-stirring mode.

The type of the antenna tested is another important attribute of the RC measurement setup. The AUTs employed in the experiments are a vertically polarized discone

(a) External view of the classical RC. *(b)* Equipment layout inside the classical RC.

Figure 4.1: RC setup for non-reference measurement methods for determining the antenna efficiency. AUT1: the discone antenna, AUT2: the dual-ridge horn antenna.

antenna working from 100 MHz to 6 GHz [40] and a standard double ridged guide horn antenna which has been designed to operate between 80 MHz and 1 GHz [41]. Both of the antennas are used as AUTs in both the one-antenna and the two-antenna approaches.

The AUTs were connected to the Keysight N5230A vector network analyzer (VNA), which was performing sweeps between 100 MHz and 6 GHz, giving 38000 frequency sampling points. For the one-antenna method, the AUT was connected to the port 1 of VNA via cables running through the bulkhead of the chamber and the S_{11} was measured (see Fig. 3.1b). For the two-antenna method, both antennas were connected to the VNA enabling two separate channels for the transmitted and received signal (see Fig. 3.1a). Before any measurement was performed, the Keysight 85033E 3.5mm calibration kit was used to calibrate the VNA. The recorded data was saved to the computer from the VNA using GPIB-USB cable and the whole setup was automated using LabVIEW software.

The control software was used to specify the steps size and the number of stirrer positions for classical RC and sampling rate for VIRC. The frequency range and the number of frequency points were specified directly in the VNA software. When the measurement was initialized, a signal was transmitted from the VNA to the AUT over the specified frequency band. The AUT induced EM modes in the chamber that interacted with the stirrer and the walls of the chambers. The LabVIEW software read the data received from AUT (second AUT, in case of two-antenna approach) and saved it for further post-processing.

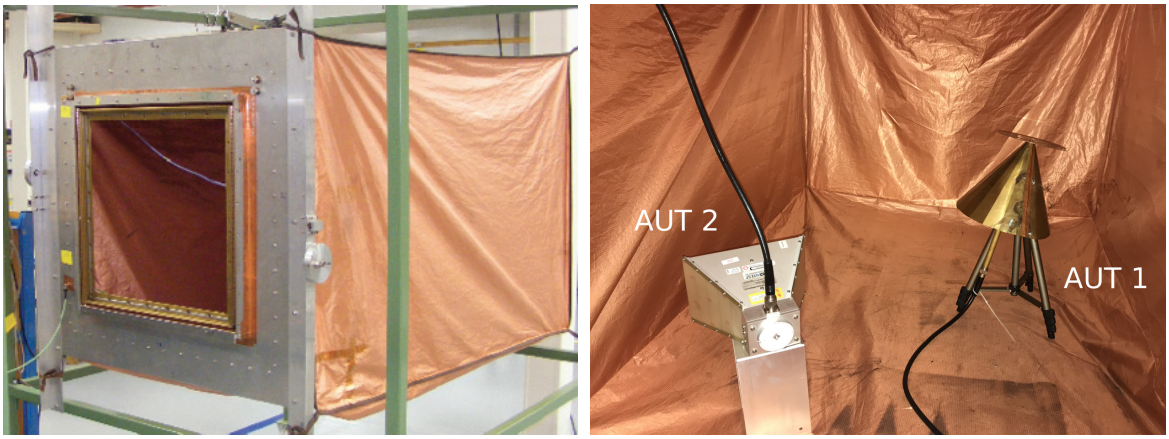

(a) External view of the VIRC. *(b)* Equipment layout inside the VIRC.

Figure 4.2: VIRC setup for non-reference measurement methods for determining the antenna efficiency. AUT1: the discone antenna, AUT2: the dual-ridge horn antenna.

4.2 Q-factor Experimental Setup

4.2.1 Frequency Domain

A series of measurements of the Q of an RC and VIRC were performed. The Q_{FD} was estimated using (2.4) based on the same measurement setup as for the antenna efficiency measurements described above. The frequency sweeps were performed on VNA within the range between 100 MHz and 6 GHz at 38000 frequency points. The LabVIEW software was used to specify the step-size of the classical RC stirrer position in a mode-tuning approach, but also to control how many sweeps are performed during VIRC measurements in a mode-stirring approach. The measurements were performed by using the 5 AUT positions within the volume sampling. In order to perform a statistical analysis, more samples can be obtained using frequency stirring with 5 MHz, 10 MHz, 20 MHz, and 50 MHz bandwidth [42]. Before using the frequency stirring technique, it is essential to verify that the data from two successive frequencies is uncorrelated. The separation of two uncorrelated points $\Delta f > f/Q$ [42], which in the case of measured environments, is at least 5 MHz [7].

4.2.2 Time Domain

As the name implies, in the time domain, the signals are analyzed with respect to time. In the reverberation chamber, generally, the excitation pulse required in the time domain measurement is short compared to the chamber time constant [14]. This was made possible by using two setups (from here referred as PDP and Direct Q_{TD} measurements).

PDP Q_{TD} measurements were made possible using a VNA with the time domain option and controlling the bandwidth of the input signal. In our measurements, the bandwidth was chosen to be 400 MHz centered at the 13 frequencies listed below. Choice of the bandwidth is made based on the volumes of the chambers [21]. The two antenna configuration like that shown in Figure 3.1a was used to obtain PDP Q_{TD}. The experimental setup was similar to the that shown in Figure 4.1b, in which a VNA was connected to two AUTs. The VNA performed a series of frequency-domain CW measurements over the desired pulse bandwidth. A discrete Fourier transform performed on the signal from the receive antenna by the VNA then yielded the time-domain response.

The experimental setup employed to measure the Direct Q_{TD} is depicted in Figure 4.3. The measurements were performed by placing a high speed and extremely accurate 3D E-field analyzer LSProbe 1.2 inside the chamber [43]. The chamber is excited with a pulse modulated sine from a Keysight E8267D PSG signal generator using the AUT. The 'on' and 'off' time of the signal have to be large compared to the chamber time constant τ_{RC}. The details on the choice of the bandwidth of the signal required to perform a measurement are found in [21] and [44].

For Q_{TD} measurements, in order to maximize the accuracy of the comparison, it is important to record subsequent samples over time with high sampling rate (2 MSamples/s burst mode sampling, in our case). In both classical RC and the VIRC, the data were collected in a similar manner, i.e., by mode-stirring, with the sole difference lying in the mechanical stirring techniques. The Q_{TD} measurements were recorded using LabVIEW at 13 frequency points: 400 MHz, 500 MHz, 600 MHz, 700 MHz, 800 MHz, 900 MHz, 1 GHz, 1.5 GHz, 2 GHz, 3 GHz, 4 GHz, 5 GHz, and 6 GHz. The selected range covers the frequencies between the lowest usable frequency (LUF) of both chambers and 6 GHz which was the highest frequency over which efficiency measurements were performed.

The idea of the method is to drive the chamber with a pulse modulated sine from the signal generator and measure the decay time of the energy within the cavity using the E-field probe. The advantage of using this probe instead of VNA is the much higher dynamic range and high-speed analog-to-digital converter used to digitize signal level. The scope mode of LSProbe was used to trigger the E-field measurements for each frequency step independently, with 2 MSamples/s burst sampling mode.

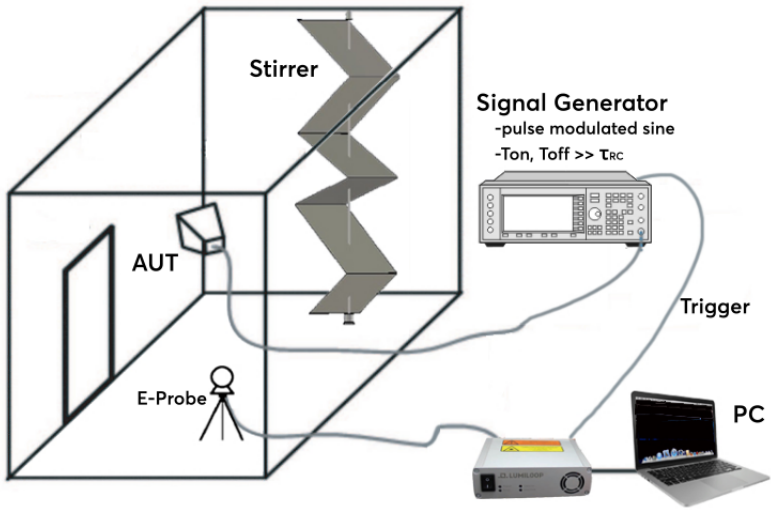

Figure 4.3: Experimental setup to measure the quality factor $\langle Q \rangle$.

4.3 Enhanced Backscatter Coefficient Experimental Setup

The two antenna configuration like that shown in Figure 3.1a is used to obtain experimental values of e_b for corresponding frequency ranges. The experimental setup was similar to the that shown in Figure 4.1b and Figure 4.2b, in which a VNA was connected to two AUTs. The expression (3.9) requires the S-parameters to have contributions from only the stirred energy in the RC and VIRC. The unstirred contribution is removed as shown in (3.7). In order to investigate the relative effect of the mismatch correction on the measured e_b, corrected S-parameters (3.8) were used in expression (3.9). This made it possible to accurately determine the e_b and analyze the uncertainty of the chambers over the frequency the measurements were performed at.

Chapter 5

Measurement Results and Analysis

5.1 RC Characterization

This chapter presents the analysis on the performed measurements to characterize spatial uniformity and compare the difference in the Q-factor measured in the frequency and time domains for both chambers. First, the characterization of spatial uniformity of the reverberation chamber is presented together with the uncertainty estimates, based on the enhanced backscatter coefficient measurements. Second, the Q-factor measurements were analyzed in order to compare two commonly used approaches to measure Q-factor and illustrate the difference between the measurements performed in RC and VIRC.

5.1.1 Spatial Uniformity and Uncertainty Estimates

Figure 5.1 shows the e_b for VIRC as a function of frequency within 200 MHz to 6 GHz. This data has been frequency stirred (averaged) with bandwidth windows of 5, 10, 20 and 50 MHz as mentioned in Section 4.2.1. As can be seen, e_b fluctuates at low frequency, then settles to a smaller variation with an average value of 2.03 and relative uncertainty close to 0.12 (for 20 MHz FS) at frequencies above 700 MHz, estimated low-frequency cutoff of the VIRC. VIRC seems to work well in terms of field uniformity above 700 MHz and not 400 MHz as was previously established in [7].

The measured e_b results for the classical RC and VIRC are shown in Figure 5.2. The first observation made is that Figures 5.2a and 5.2b are virtually identical. This is an expected result since the efficiency terms, including mismatch, cancel when calculating e_b using (3.9). Also, it is seen that frequency stirring greatly decreases the spread of the measured results for both cases. The e_b of the two chambers in the frequency range between 200 MHz and 2200 MHz was examined. It is noticed that the field of VIRC at lower frequencies show slightly better uniformity than those in classical RC as its e_b is closer to 2. We see that e_b is close to 2 at the high-frequency end for both cases and

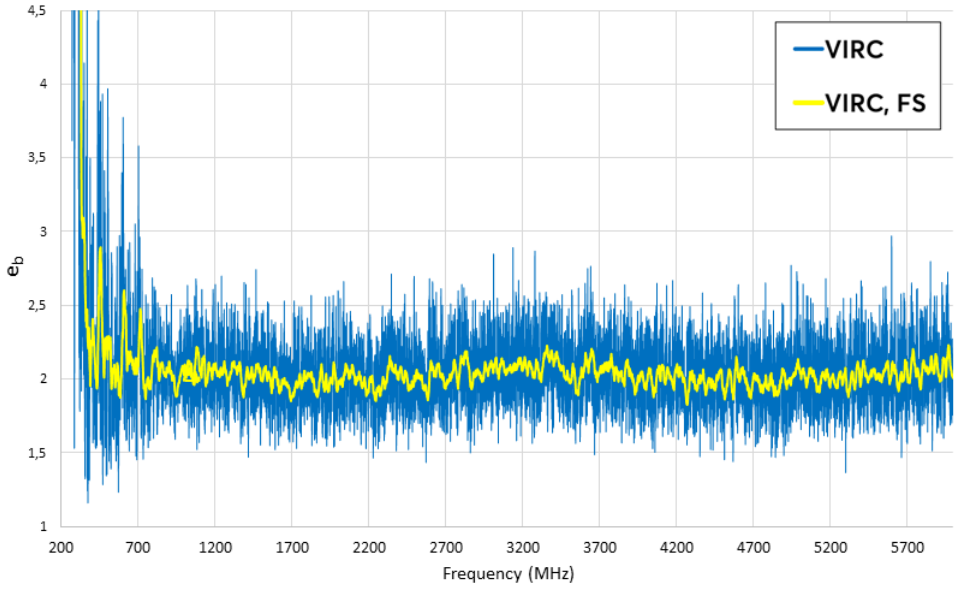

Figure 5.1: Enhanced backscatter coefficient e_b of VIRC computed from the two-antenna setup. Yellow line indicates the 20 MHz frequency stirring (FS).

the obtained values are virtually identical. Larger deviations from 2 at lower-frequency end are observed for both cases.

Based on the obtained e_b values, it is useful to plot the average uncertainty over the entire frequency span as a function of the number of frequency samples used to obtain the uncertainty estimate. Figure 5.3a illustrates the relative uncertainty computed from e_b for both classical RC and VIRC, using two-antenna setup. The black (classical RC) and yellow (VIRC) lines illustrate the data obtained from 20 MHz frequency stirring. Frequency stirring decreases the uncertainty for both cases and greatly decreases the spread of the obtained results. The relative uncertainty of the VIRC is slightly lower than the $\widehat{\widetilde{u}}_{e_b}$ of classical RC over low frequencies, the $\widehat{\widetilde{u}}_{e_b}$ estimation over the rest of frequency range is pretty much the same.

From the plots of e_b and $\widehat{\widetilde{u}}_{e_b}$ it is apparent that frequency stirring gives mixed results. At frequencies less than roughly 700 MHz, the error increases making any result completely useless. However, at frequencies greater than 700 MHz frequency stirring effectively reduces the error. This decrease in uncertainty is related to the amount of correlation between the collected samples, both in frequency and over different antenna efficiency positions [39].

The accuracy of the measurements can be estimated by calculating the relative uncertainty of the e_b around its estimated mean value for different frequency smoothing windows sizes. The calculates results obtained from the curves in Figure 5.2 are shown in Table 5.1.

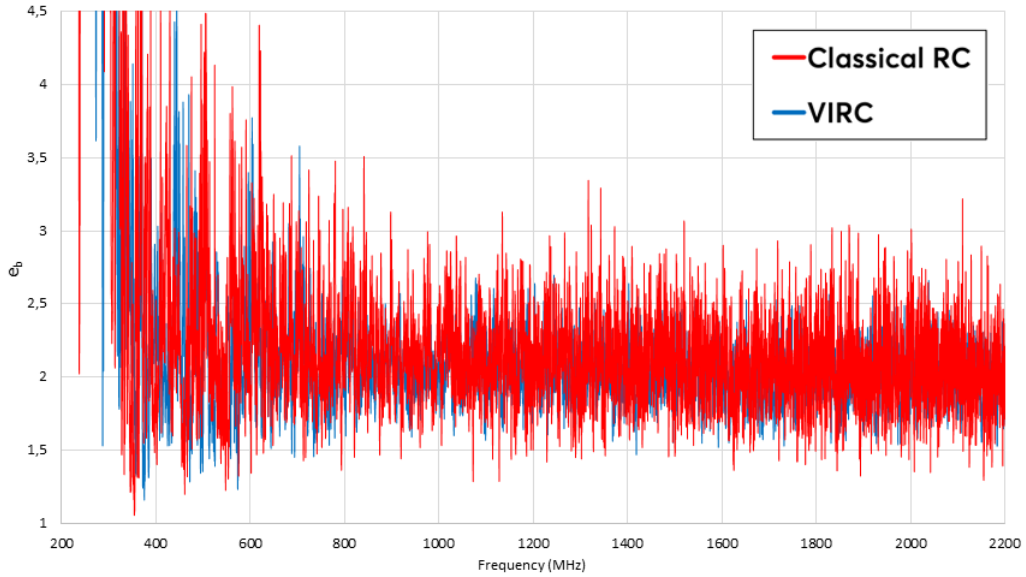

(a) No frequency stirring and no mismatch correction.

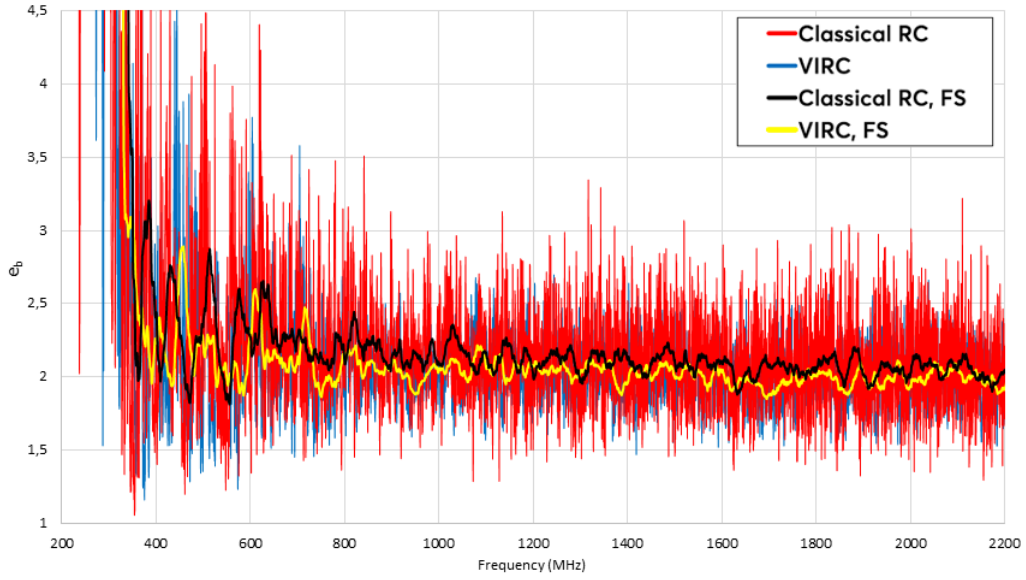

(b) Mismatch correction, with frequency stirring bandwidth 20 MHz.

Figure 5.2: Enhanced backscatter coefficient e_b for both classical RC and VIRC.

Table 5.1: Relative uncertainty for different frequency smoothing windows sizes.

Chamber	**Size [m]**	**Frequency [GHz]**	$\widehat{\widetilde{u}}_{e_b}$ for 20MHz **min-max**	$\widehat{\widetilde{u}}_{e_b}$ for 50MHz **min-max**
Classical RC	1.5 x 1.3 x 1	0.7 - 6	0.17 - 0.32	0.1 - 0.21
VIRC	1.5 x 1.2 x 1	0.7 - 6	0.12 - 0.28	0.07 - 0.21

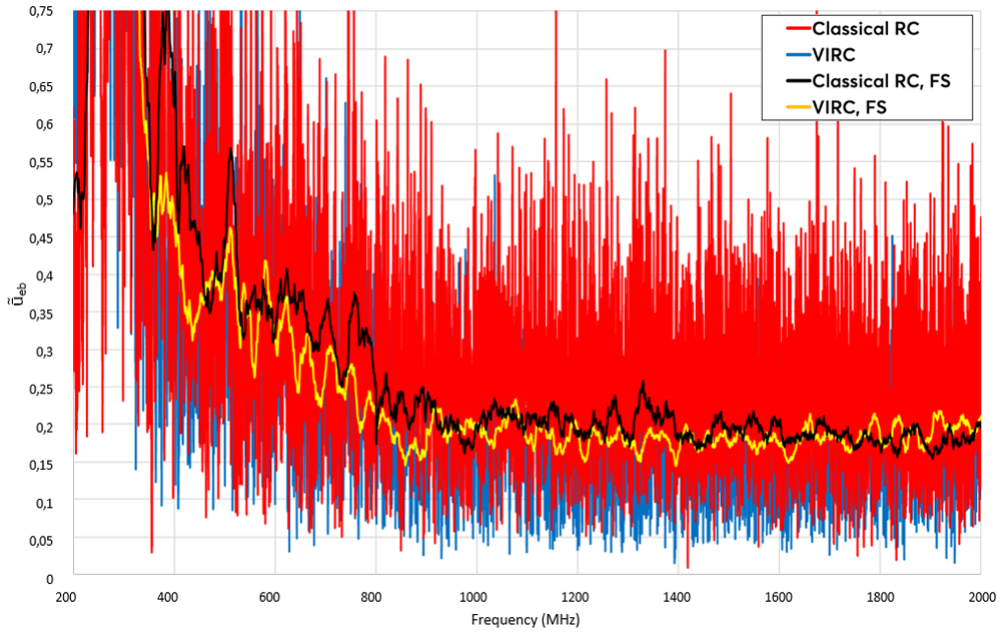

(a) Relative uncertainty computed from e_b, 20MHz frequency stirring.

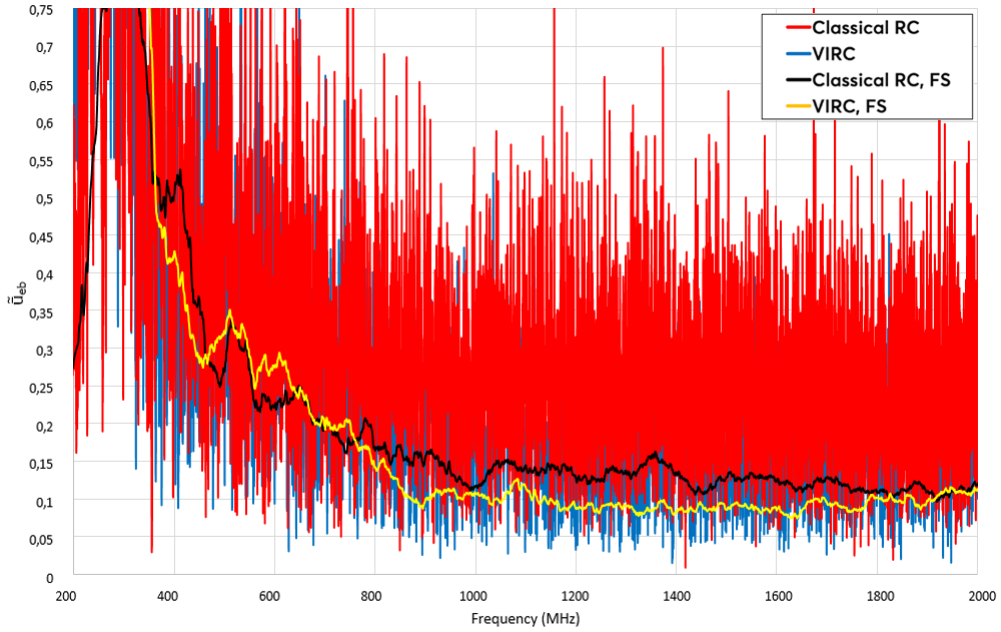

(b) Relative uncertainty computed from e_b, 50MHz frequency stirring.

Figure 5.3: Relative uncertainty computed from e_b of classical RC and VIRC using two-antenna setup. Black and yellow lines corresponds to data obtained using frequency stirring.

Moreover, with larger frequency stirring window (see Fig.5.3b) the minimum uncertainty is 0.07 for VIRC, which requires all collected samples to be uncorrelated. The obtained $\widehat{\widetilde{u}}_{e_b}$ for both cases was processed with 20 MHz moving average filter and used

in the next section to calculate the measured total and radiation efficiency.

5.1.2 Quality Factor

In order to analyze the discrepancy between the frequency domain and time-domain Q factors, measurements were performed in both reverberation chambers. The assumption of similarity regarding the volumes of the classical RC and the VIRC were validated by looking at the corresponding average, composite Q factors, calculated directly in the time domain, as described in [23].

Table 5.2: Measured Q-factors in Classical RC using Frequency and Time Domain.

Frequency [MHz]	Q_{FD}, **[dB]**	Q_{TD}, **[dB]**	**Difference, [dB]**	$\widehat{\widetilde{u}}_{\Delta P_{r\|dB}}$
400	30.54	31.60	1.06	0.38
500	31.18	32.22	1.03	0.36
600	31.06	32.50	1.43	0.32
700	31.50	32.36	0.85	0.13
800	31.77	32.98	1.21	0.12
900	32.98	33.47	0.49	0.11
1000	33.29	34.09	0.81	0.08
1500	37.21	38.25	1.03	0.08
2000	40.44	41.98	0.73	0.08
3000	42.46	43.04	0.60	0.07

The frequency domain Q-factor of classical RC (see Section 2.2) was determined over multiple frequency steps from 400 MHz to 6 GHz. The PDP (power delay profile) and τ_{RC} (chamber time constant) were determined over a bandwidth of 20 MHz. In Figure 5.4 the Q-factor is plotted as a function of frequency for various loading conditions. It can be seen that, as expected, the absorbers significantly reduce the Q-factor since power is absorbed in the load. These measurements were performed in order to analyze how chamber would act if the losses in the chamber are not dominated by the chamber walls and to determine a threshold quality factor Q_{thr} for further chamber characteristics analysis [45]. For an efficient or effective reverberation chamber, the Q should exceed this threshold value. Also, the Q_{FD} obtained for classical RC is used to analyze the difference between the Q_{TD} measurements, performed as described in Section 4.2.2.

The Q-factor values measured at different operating frequencies through both frequency domain (2.4) and time domain (2.9) techniques are tabulated in Table 5.2. The frequency domain Q values are averaged over a finite bandwidth, equivalent to adding

frequency stirring to supplement the intended source stirring (see Section 4.2.1). The Q values reported for time domain are calculated using the method in Section 4.2.2. The Q values measured using Q_{TD} method are higher than those found with the CW method under all conditions in Table 5.2. These results corroborate the results presented in [10] and [14]. Table 5.2 also provides the uncertainty estimates for the Direct Q_{TD} (based on (2.9)) as a function of frequency in considered cases in Figure 5.5. The Direct Q_{TD} measurements performed in both chambers, show that for an unloaded chamber the $\widehat{\widetilde{u}}_{\Delta P_{r|dB}}$ is between 0.38 - 0.07 for the bandwidth 0.4 - 6 GHz (the higher the frequency, the smaller the $\widehat{\widetilde{u}}_{\Delta P_{r|dB}}$). It is of interest to compare the performance of the classical RC to the results obtained in VIRC ($\widehat{\widetilde{u}}_{\Delta P_{r|dB}}$ is between 0.41 - 0.08 for the same bandwidth). From Tables 5.2 and 5.3 it is clear that the VIRC has slightly larger $\widehat{\widetilde{u}}_{\Delta P_{r|dB}}$ and thus a slightly worse performance for similar loading (similar average mode bandwidth). This result is expected, because of the slight difference in volume between the two analyzed reverberant environments. However, the comparison also shows that the performance of VIRC is similar to classical RC over the considered frequency span.

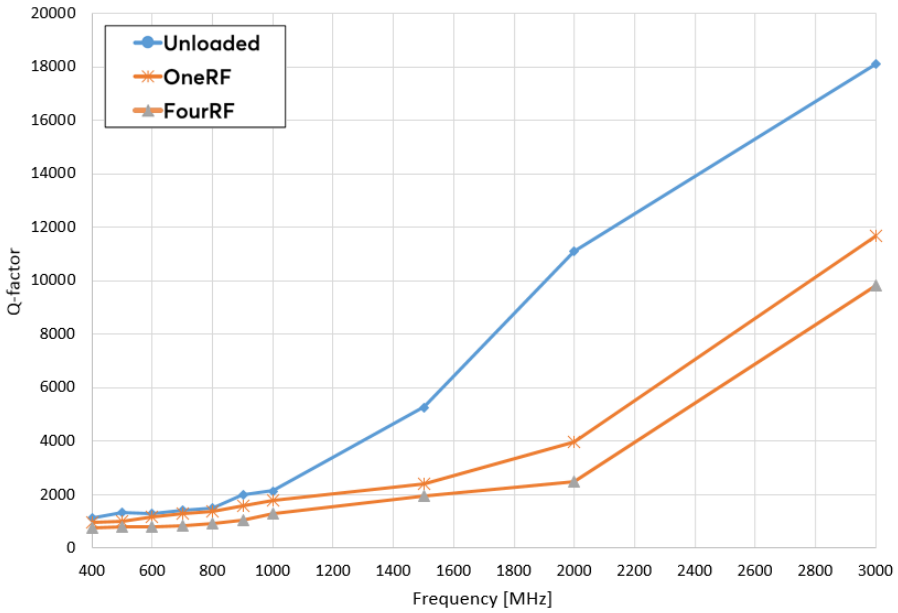

Figure 5.4: The quality factor Q measured in Classical RC as a function of frequency. The different curves represent different loading configurations.

Measured composite Q-factors for both unloaded classical RC and VIRC are presented in Figure 5.5. As seen in Figure 5.5, the results of both chambers are similar up to 1 GHz, and the consistency of Q-factors is maintained. This is in agreement with the [7], which implied that both chambers are indeed comparable. Above 1 GHz, an increasing difference is visible, this is due to the fact that the thick walls of the RC have higher shielding effectiveness as opposed to the thin flexible material of VIRC. Measured values are used in Section 5.2 to calculate the measured total and radiation

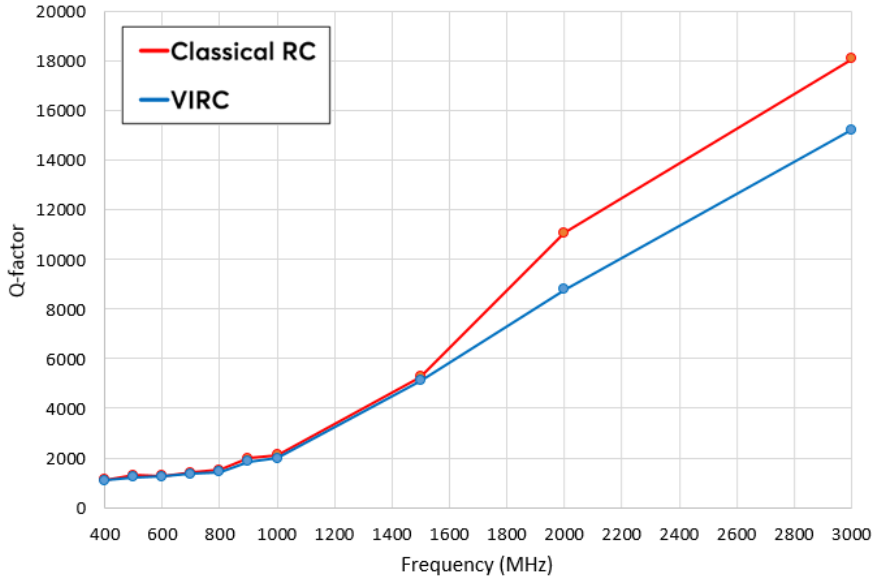

Figure 5.5: Average Q-factors of the unloaded Classical RC and VIRC.

efficiencies of the AUTs.

Time domain Q-factor measurements were performed with VIRC using the method explained above in Section 4.2.2. Figure 5.6 shows the measured slopes averaged over different positions of the tuner (the curves have been shifted on the time axis in order to clarify the illustration). Figure 5.6 presents the average traces for different numbers of stirrer (tuner) positions (N= 1, 2, 3, 5, 10, 15, 50) for a frequency near the chamber LUF.

The theory presented in Chapter 2 assumes that measurement samples are i.i.d., i.e., an ideal RC is assumed. However, to achieve a well-stirred the RC measurements, many samples should be collected to perform the statistical analysis. An effective stirring process will produce highly independent samples (low correlation). If enough statistically independent samples can be obtained, then the average of the power measured at any location within the working volume of the RC will be constant (within some standard deviation) and the RC is said to be spatially uniform [14]. For the best, direct comparison of Q-factors, 50 samples (i.e., the expected amount of i.i.d samples in RC [7]) were uniformly picked from both datasets for the analysis.

From Table 5.3 it is shown that there is negligible difference between the PDP Q_{TD} and Direct TD estimated Q for VIRC. The Direct Q_{TD} values are only slightly higher than those found using the PDP approach and are within statistical uncertainty for a reverberation chamber measurement. The similarity in Q between the Direct and PDP TD measurements show that Direct Q_{TD} approach may be valid for estimating the Q of various reverberant environments, such as a continuously shaking VIRC, where the measurement is much faster than the rate of change of the field.

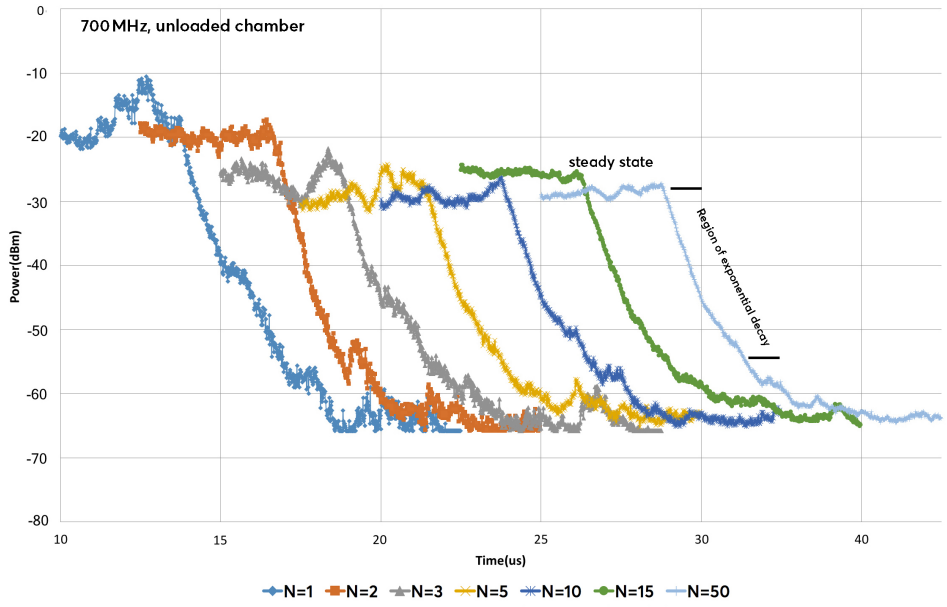

Figure 5.6: Typical traces of the received power for different tuner positions. After the exiting signal is switched off, an exponential decay can be observed in the averaged trace.

Table 5.3: Measured Q-factors in VIRC using Time Domain.

Frequency [MHz]	PDP Q_{TD}, [dB]	Direct Q_{TD}, [dB]	**Difference**, [dB]	$\widehat{\widehat{u}}_{\Delta P_{r\|dB}}$
400	30.54	31.22	0.68	0.41
500	30.89	31.34	0.45	0.34
600	30.96	31.58	0.62	0.36
700	31.84	32.06	0.22	0.14
800	32.05	32.45	0.4	0.14
900	32.98	33.17	0.49	0.11
1000	33.26	33.69	0.19	0.1
1500	36.31	36.87	0.43	0.1
2000	38.54	39.46	0.56	0.1
3000	40.86	41.94	1.08	0.08

As illustrated in Figure 5.6, typical traces for different tuner positions, can be divided into two distinct phases, the pre-reverberant phases (shown in Fig. 5.6 as "Steady State") where energy is being distributed across resonant modes within the chamber and reverberant phase (illustrated in Fig. 5.6 as "Region of exponential decay") where the energy level exponentially decays due to losses. The losses can be due to conductive losses on the walls, the stirrer, and other objects within the chamber

including cables and the antennas. Losses also can be present due to leakage from imperfect shielding of the enclosure, and loading by the signal-source AUT and second AUT (if included).

The advantage of this technique is that the aforementioned pre-reverberant phase can be eliminated through time-gating, leaving only the reverberant field [23]. This should improve the quality of response and remove errors due to mismatch. After reducing the unwanted time domain responses, the exponential decay of the reverberant field can be used to estimate the Q of the cavity using (2.9).

5.2 Antenna Efficiency Measurements

Using the various concepts discussed in previous chapters, the antenna efficiencies were measured by using two non-reference antenna methods in both reverberation chambers. Since two antennas were used in the performed tests, we can use the data to work out the efficiencies by using both the one-antenna (3.3) and two antenna methods (3.4). Same data was used to compute the e_b (3.9) and the relative uncertainty (3.11) of the measurements. The following shows the computation performed from the measured data that ultimately lead to an estimate of total and radiation efficiencies.

First, the effect of the reflections of the reverberation chambers on the performance of the antennas has been investigated. The S parameter S_{11} was measured in both reverberation chambers and the anechoic chamber at the University of Twente. The comparison in the Figure 5.7 confirmed that S_{11} measured in a reverberation chamber (averaged over the different independent samples obtained from paddle and frequency averaging, or $\langle|S_{11,s}|^2\rangle$) was equivalent to S_{11} measurement performed in an anechoic chamber (i.e., a free-space measurement, or S_{11}). It can be seen that although two reverberation chambers have different mechanical and electrical properties, the measured intrinsic properties of the antennas agree fairly well.

Figure 5.8 shows the $\langle|S_{21,s}|^2\rangle$ measured in the two chambers. The close agreement between the RC and VIRC indicated the power losses between the two chambers are similar. Included in this plot are also mismatched corrected traces computed using (3.8). As shown the mismatch corrected traces are more linear on the dB scale at the upper frequencies, corresponding to an exponential decrease in the stirred power with frequency.

Figure 5.9 illustrate the radiation efficiencies of the discone and horn antennas used as an AUT, by using both one- and two-antenna methods in both chambers, i.e., correcting for antenna mismatch in the S-parameters. The data are smoothed over 20 MHz to show the difference between the methods and chambers more clearly. The observed relatively sharp decrease in radiation efficiencies at low frequencies is an indication that all of the RC techniques fail to accurately estimate the efficiency at those

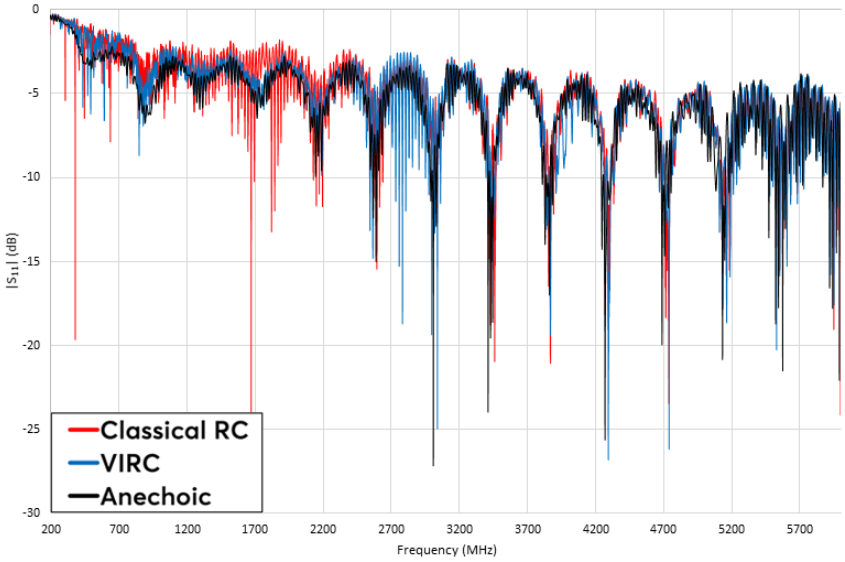

(a) AUT1: the discone antenna.

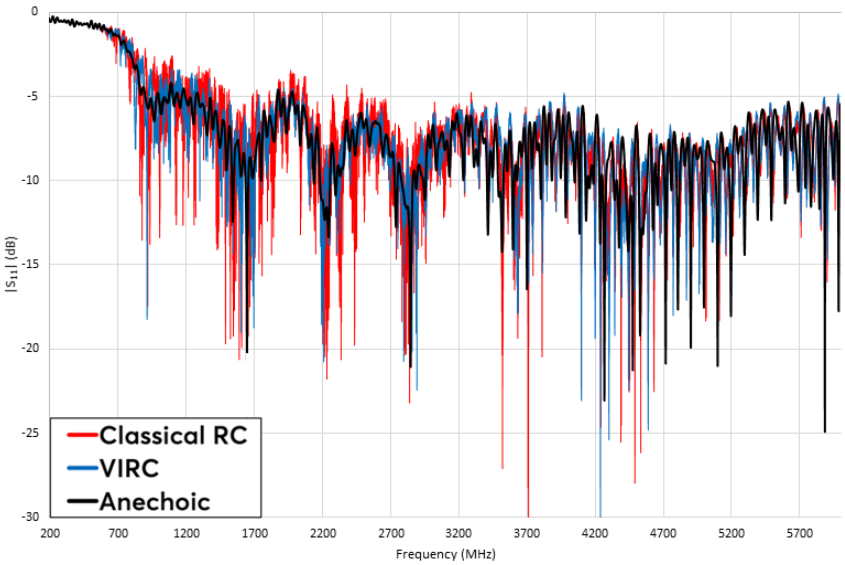

(b) AUT2: the dual-ridge horn antenna.

Figure 5.7: Reflection coefficient $|S_{11}|$ for both AUTs in free space, in the Classical RC with averaging and in the VIRC with averaging.

frequencies. However, above 700 MHz the results obtained from both chambers have a close agreement between results computed using non-reference antenna methods. For both AUTs, classical RC's one-antenna method gives slightly higher efficiencies than the two-antenna method, but VIRC's two non-reference methods agree very well. This is because the enhanced backscatter coefficients of VIRC at the test locations are slightly more close to 2 than those of classical RC as already shown in Figure 5.2 (b).

For AUT1: discone antenna (in Fig. 5.9a), VIRC has a very close agreement

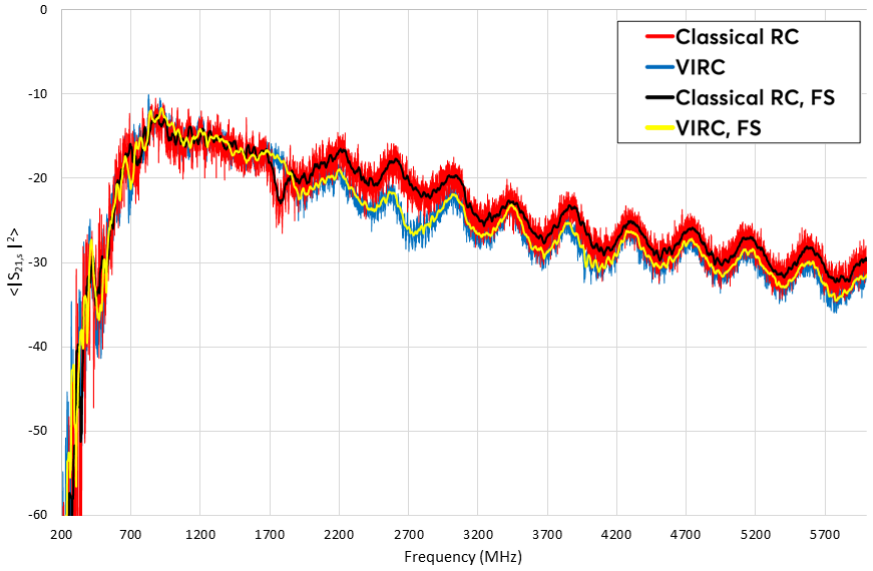

(a) No mismatch correction, with frequency stirring bandwidth 20 MHz.

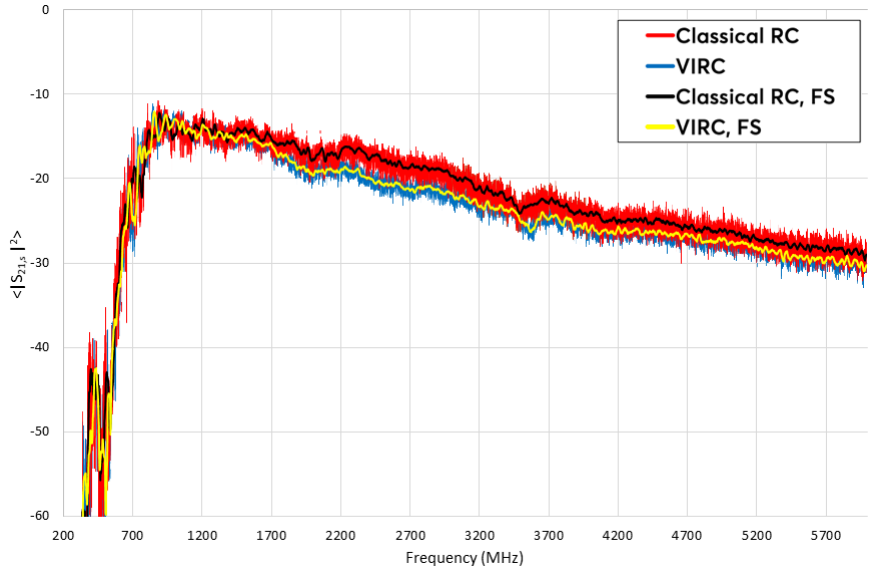

(b) Mismatch correction, with frequency stirring bandwidth 20 MHz.

Figure 5.8: Mean transferred power measured between the discone and the dual-ridge horn antenna in both chambers.

between the results calculated by using both one- and two-antenna methods for frequencies above 700 MHz but classical RC's one-antenna and two antenna methods provide a relatively larger difference in the efficiencies. For both AUTs, classical RC's one-antenna method gives slightly higher efficiencies than the two-antenna method, but VIRC's two non-reference methods agree very well. This is because the enhanced backscatter coefficients of VIRC at the test locations are more close to 2 than those of classical RC as already shown in Figure 5.2. However, classical RC's two-antenna

method provides close agreement (<5%) on antenna AUT2 (in Fig. 5.9b) and slightly poorer agreement (12%) on AUT1 with VIRC's both one- and two-antenna methods. Slight difference between these results is expected since the VIRC has a slight difference in volume compared to the classical RC.

Table 5.4: Uncertainties for the measured two antenna efficiency method cases.

		Classical RC		**VIRC**	
		STD, **[dB]**	$\widehat{\widehat{u}}_C$	STD, **[dB]**	$\widehat{\widehat{u}}_C$
Radiation	AUT1	0.3 (6.8%)	0.07	0.47 (11%)	0.12
Efficiency	AUT2	0.19 (4.3%)	0.05	0.28 (6.4%)	0.08
Total	AUT1	0.22 (5%)	0.06	0.2 (4.6%)	0.07
Efficiency	AUT2	0.21 (4.8%)	0.07	0.33 (7.5%)	0.08

By not correcting for the mismatch between the antenna feed and the cable, the total efficiency can be determined. Figure 5.11 shows the total efficiency determined from the different techniques for both antennas. These results show the classic oscillations seen in results when the mismatch is present. These results also illustrate close agreement between measured total efficiencies calculated using non-reference antenna methods, and once again prove that VIRC can be used as an alternative facility for antenna efficiency measurements.

Aside from the use of e_b and Q_{TD} as a quantity for characterizing the uncertainty of measurements conducted in both reverberation chambers, it is of interest to compare the performance of the both reverberation chambers to the standard deviation (STD) results obtained from S_{21}. In order to directly compare the $\widehat{\widehat{u}}_C$ (combined relative uncertainty of $\widehat{\widehat{u}}_{e_b}$ and $\widehat{\widehat{u}}_{\Delta P_{r|dB}}$, as defined in [46]) and STD results, the STD was computed as described in [15]. When the standard deviation is known, we can transfer this to an approximate decibel value by using [47]

$$\mathrm{STD}_{dB} = 5\log(\frac{1+\sigma}{1-\sigma}) \tag{5.1}$$

Comparing the results in Table 5.4, the observation that can be made is the similarity between $\widehat{\widehat{u}}_C$ and STD. The uncertainty comparison shows that measurements of the e_b can be used as a method for characterizing the uncertainties of the RC and VIRC. The uncertainty, $\widehat{\widehat{u}}_C$, is different from STD in that it includes the effects of the transmitted and reflected powers in the RC measurement. The drawback is that it has to be done with a VNA to obtain the reflection data, and it still requires measurements at many locations within the RC.

Additional improvements are needed in order to obtain satisfying results for low

frequencies and different loading. This could include employing position and/or polarization stirring. Also, for VIRC a reasonable solution to increase the number of independent samples and thus the accuracy is portable stirrers [7]. Also, frequency stirring would increase the accuracy, at the expense of frequency resolution.

In addition, the values of relative uncertainty estimate (obtained from e_b), shown in Section 5.1.1 are used to give confidence interval for antenna efficiency measurements for both chamber.

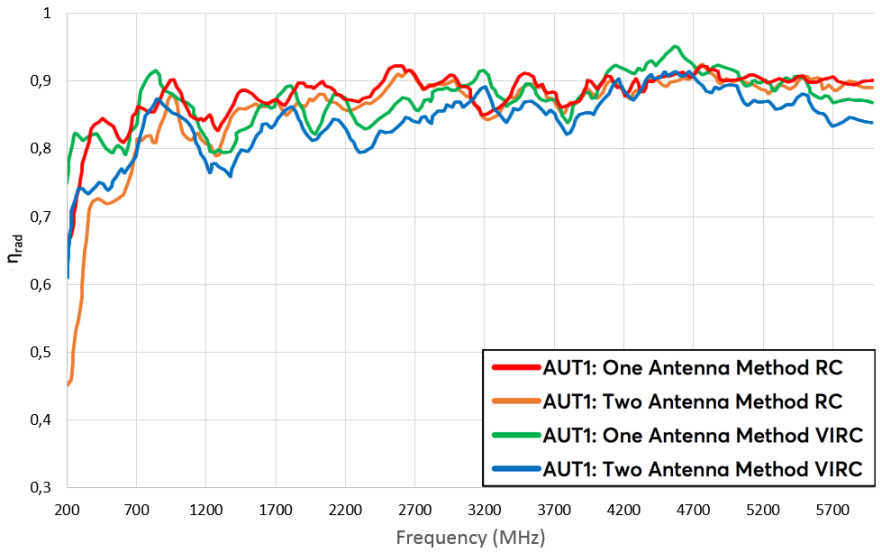

(a) AUT1: the discone antenna.

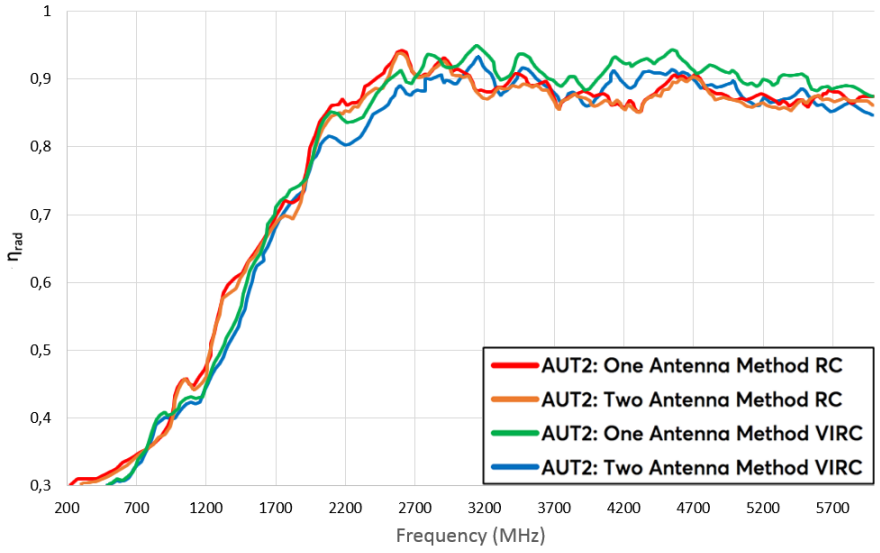

(b) AUT2: the dual-ridge horn antenna.

Figure 5.9: Comparing radiation efficiencies of the AUTs obtained by using both one-antenna and two-antenna methods.

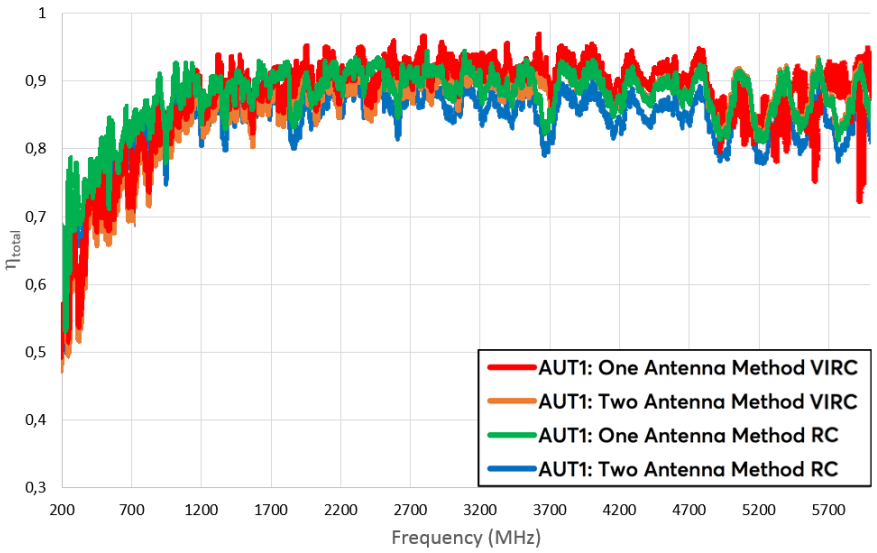

(a) AUT1: the discone antenna.

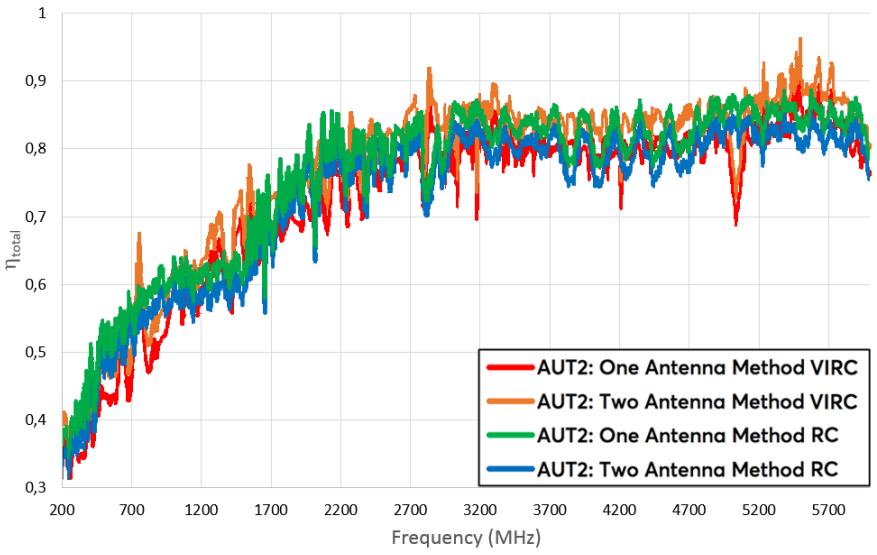

(b) AUT2: the dual-ridge horn antenna.

Figure 5.10: Comparing total efficiencies of the AUTs obtained by using both one-antenna and two-antenna methods.

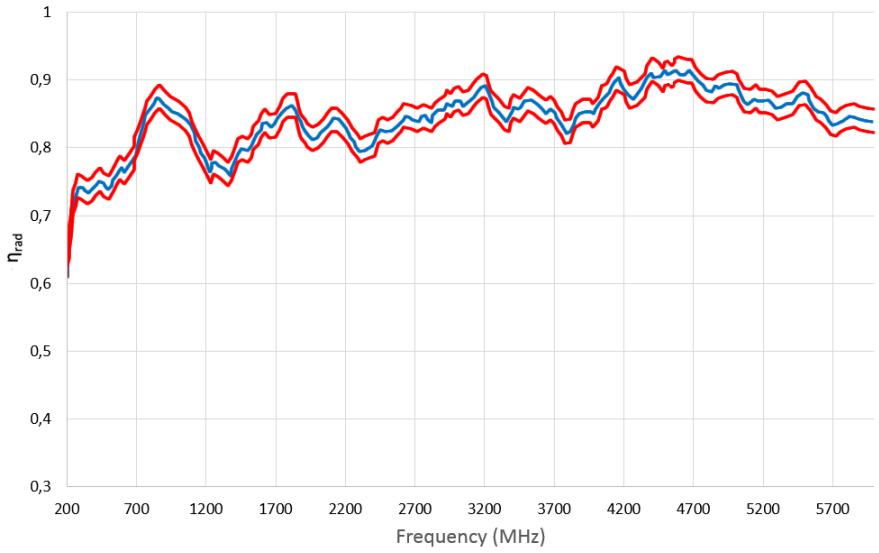

(a) Radiation Efficiency Confidence Interval.

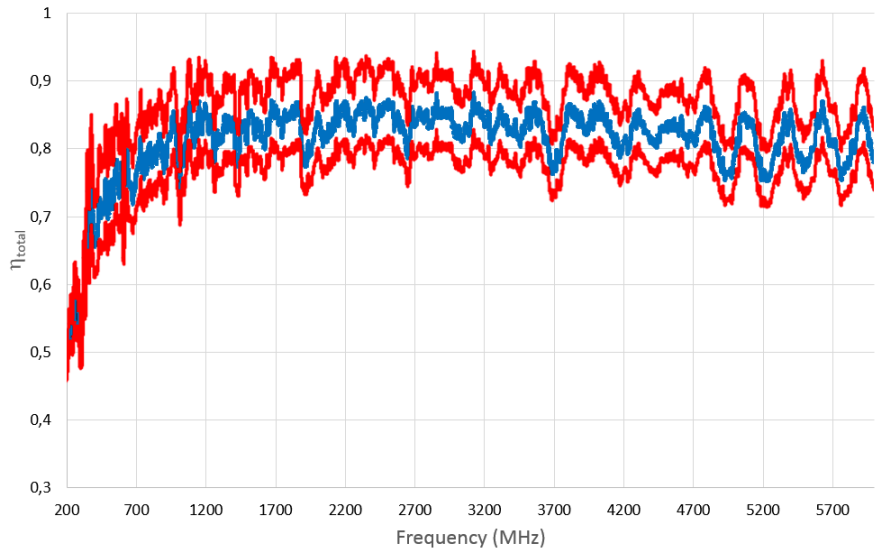

(b) Total Efficiency Confidence Interval.

Figure 5.11: Confidence interval for the total and radiation efficiency results of the discone antenna computed using non-reference two-antenna method.

Chapter 6

Conclusions and Future Work

In this thesis, we investigated the possible usage of VIRC for antenna efficiency measurements. The total and radiation antenna efficiencies measured in two different RCs for two wide-band antennas were compared. The antenna efficiencies were measured by using two non-reference antenna methods namely one-antenna method and two-antenna method in the reverberation chambers at the University of Twente, Enschede, the Netherlands. Analyzed results show that performance of VIRC is similar to classical RC over the considered frequency span. It has been found that although the two chambers differ in dimensions and stirring configuration and hence in Q-factors and enhanced backscatter coefficients, the radiation efficiencies of the antennas measured using the two-antenna method between two RCs agree fairly well with slightly better agreement for the discone antenna than for dual-ridged horn antenna.

An overview of the RC was given that compared it to other types of measurement facilities and the advantages and limitations of the RC were discussed. Of particular concern was the statistical distribution of samples measured in the RC, which has been shown to be related to the frequency of operation, the relative size of the RC and of the internal objects, and the effectiveness of the stirring method employed. The spatial uniformity of the chambers was studied using the variation of enhanced backscatter coefficient over a relatively small bandwidth of frequencies. The measured values were used to obtain the relative uncertainty caused by spatial dependence. It has been shown that the enhanced backscatter coefficient is a useful quantity for characterization of the reverberation chambers. By observing the variation of e_b over multiple antenna configurations, the spatial variation of the reverberant environment was determined in a similar manner to insertion loss variation. Many of the concepts formulated and discussed in earlier chapters were used to compute the total efficiencies of a discone and dual-ridge horn antennas. The efficiency estimation results were compared with results from classical RC. Measurements have shown that the VIRC may be used as an alternative testing facility for antenna efficiency measurements and non-reference antenna methods can be performed accurately. This statement has been verified by

confirming very low measurement uncertainties and close agreement between calculated results using non-reference antenna methods.

In future work, a further study into VIRC and measurement procedures associated with it, aimed at smoothing the transition into a fully standardized and accepted facility within the measurement industry can be performed. Of particular interest is a study of the estimated radiation efficiency when the field distribution might not be uniform. The results in both chambers may be compared to the case when uniformity is assumed. A mathematical/physical model describing the influence of the field non-uniformity on the measured antenna efficiency can be produced. In addition, the interactions with different measurement environments that result in a different performance of the tested antenna systems can be investigated. For example, the MIMO (Multiple-Input Multiple-Output) antenna efficiency is sensitive to both the radiation efficiency of tested antennas, the reference antennas as well as the wave field distribution in the testing environment. These effects may be further studied in both chambers to make VIRC accepted alternative testing facility for OTA characterization of wireless devices.

Bibliography

[1] W. P. Kodali, *Engineering Electromagnetic Compatibility: Principles, Measurements, Technologies, and Computer Models*. Wiley-IEEE Press, 2001.

[2] F. Leferink, J. Boudenot, and W. van Etten, "Experimental results obtained in the vibrating intrinsic reverberation chamber," in *IEEE International Symposium on Electromagnetic Compatibility. Symposium Record (Cat. No.00CH37016)*, vol. 2, Aug 2000, pp. 639–644 vol.2.

[3] F. Leferink and W. van Etten, "Optimal utilization of a reverberation chamber," in *Euro EMC 2000, Symposium on EMC, Brugge*, 2000, pp. 201–206.

[4] N. K. Kouveliotis, P. T. Trakadas, and C. N. Capsalis, "FDTD modeling of a vibrating intrinsic reverberation chamber," in *Progress In Electromagnetics Research, Vol. 39*, 2003, pp. 47–59.

[5] S. van de Beek, R. Vogt-Ardatjew, H. Schipper, and F. Leferink, "Vibrating intrinsic reverberation chambers for shielding effectiveness measurements," in *International Symposium on Electromagnetic Compatibility - EMC EUROPE*, Sept 2012, pp. 1–6.

[6] F. Leferink, D. J. G. Boerle, and F. A. G. Sogtoen, "In-situ EMI measurement using a vibrating reverberation chamber," 2002.

[7] R. Vogt-Ardatjew, "Electromagnetic fields in reverberant environments," Ph.D. dissertation, University of Twente, 2017.

[8] R. Vogt-Ardatjew, S. van de Beek, and F. Leferink, "Experimental extreme field strength investigation in reverberant enclosures," in *2014 International Symposium on Electromagnetic Compatibility*, Sept 2014, pp. 332–336.

[9] A. A. Glazunov, V.-M. Kolmonen, and T. Laitinen, *MIMO Over-The-Air Testing*. Wiley-Blackwell, 2012, ch. 15, pp. 411–441.

[10] C. L. Holloway, H. A. Shah, R. J. Pirkl, W. F. Young, D. A. Hill, and J. Ladbury, "Reverberation chamber techniques for determining the radiation and total

efficiency of antennas," *IEEE Transactions on Antennas and Propagation*, vol. 60, no. 4, pp. 1758–1770, April 2012.

[11] R. F. Harrington, *Time-Harmonic Electromagnetic Fields.* Wiley-IEEE Press, 2001.

[12] C. A. Balanis, *Advanced Engineering Electromagnetics.* Wiley, 1989.

[13] J. D. Kraus, *Electromagnetics (Mcgraw-Hill Series in Electrical Engineering. Electromagnetics).* Mcgraw-Hill College, 1991.

[14] D. A. Hill, *Electromagnetic Fields in Cavities: Deterministic and Statistical Theories.* Wiley-IEEE Press, 2009.

[15] C. R. Dunlap, "Reverberation chamber characterization using enhanced backscatter coefficient measurements," Ph.D. dissertation, University of Colorado, 2013.

[16] M. L. Crawford and G. H. Koepke, "Design, evaluation, and use of a reverberation chamber for performing electromagnetic susceptibility/vulnerability measurements," *U.S. Nat. Bur. Stand. Tech. Note 1092*, 1986.

[17] J. M. Ladbury, G. Koepke, and D. Camell, "Evaluation of the NASA Langley Research Center mode-stirred chamber facility," *Nat. Inst. of Standards and Technology Tech.Note 1508, Boulder, CO, USA,*, 1999.

[18] E. Genender, C. L. Holloway, K. A. Remley, J. M. Ladbury, G. Koepke, and H. Garbe, "Simulating the multipath channel with a reverberation chamber: Application to bit error rate measurements," *IEEE Transactions on Electromagnetic Compatibility*, vol. 52, no. 4, pp. 766–777, Nov 2010.

[19] *"Test and Measurement techniques-Reverberation Chamber Test Methods"*. Electromagnetic Compatibility Part 4-21.

[20] R. E. Richardson, "Reverberent microwave propagation," *Naval Surface Warefare Center-Dahlgren Division, Dahlgren, Virginia, 22448-5100,Tech. Rep. NSWCDD/TR-08/127*, 2008.

[21] V. Rajamani, C. F. Bunting, and J. C. West, "Differences in quality factor estimation in frequency and time domain," in *2012 Asia-Pacific Symposium on Electromagnetic Compatibility*, 2012, pp. 505–508.

[22] C. L. Holloway, H. A. Shah, R. J. Pirkl, K. A. Remley, D. A. Hill, and J. Ladbury, "Early time behavior in reverberation chambers and its effect on the relationships between coherence bandwidth, chamber decay time, RMS delay spread, and

the chamber buildup time," *IEEE Transactions on Electromagnetic Compatibility*, vol. 54, no. 4, pp. 714–725, Aug 2012.

[23] H. G. Krauthauser, "On the measurement of total radiated power in uncalibrated reverberation chambers," *IEEE Transactions on Electromagnetic Compatibility*, vol. 49, no. 2, pp. 270–279, May 2007.

[24] P. Corona, G. Latmiral, and E. Paolini, "Performance and analysis of a reverberating enclosure with variable geometry," *IEEE Transactions on Electromagnetic Compatibility*, vol. EMC-22, no. 1, pp. 2–5, Feb 1980.

[25] A. A. Glazunov, J. Carlsson, and C. P. Lötbäck, "Reverberating dreams-the story of an OTA chamber," in *2017 IEEE International Symposium on Antennas and Propagation USNC/URSI National Radio Science Meeting*, July 2017, pp. 239–240.

[26] P. S. Kildal and K. Rosengren, "Correlation and capacity of MIMO systems and mutual coupling, radiation efficiency, and diversity gain of their antennas: simulations and measurements in a reverberation chamber," *IEEE Communications Magazine*, vol. 42, no. 12, pp. 104–112, Dec 2004.

[27] S. J. Boyes, P. J. Soh, Y. Huang, G. A. E. Vandenbosch, and N. Khiabani, "Measurement and performance of textile antenna efficiency on a human body in a reverberation chamber," *IEEE Transactions on Antennas and Propagation*, vol. 61, no. 2, pp. 871–881, Feb 2013.

[28] H. G. Krauthauser and M. Herbrig, "Yet another antenna efficiency measurement method in reverberation chambers," in *2010 IEEE International Symposium on Electromagnetic Compatibility*, July 2010, pp. 536–540.

[29] C. Li, T. Loh, Z. H. Tian, Q. Xu, and Y. Huang, "A comparison of antenna efficiency measurements performed in two reverberation chambers using non-reference antenna methods," in *2015 Loughborough Antennas Propagation Conference (LAPC)*, Nov 2015, pp. 1–5.

[30] K. Rosengren, P. S. Kildal, J. Carlsson, and O. Lunden, "A new method to measure radiation efficiency of terminal antennas," in *2000 IEEE-APS Conference on Antennas and Propagation for Wireless Communications (Cat. No.00EX380)*, Nov 2000, pp. 5–8.

[31] G. L. Fur, C. Lemoine, P. Besnier, and A. Sharaiha, "Performances of UWB Wheeler cap and reverberation chamber to carry out efficiency measurements of narrowband antennas," *IEEE Antennas and Wireless Propagation Letters*, vol. 8, pp. 332–335, 2009.

[32] A. Hussain, A. A. Glazunov, B. Þ. Einarsson, and P. Kildal, "Antenna measurements in reverberation chamber using USRP," *IEEE Transactions on Antennas and Propagation*, vol. 64, no. 3, pp. 1152–1157, March 2016.

[33] A. Hussain, P. Kildal, and A. A. Glazunov, "Interpreting the total isotropic sensitivity and diversity gain of LTE-enabled wireless devices from over-the-air throughput measurements in reverberation chambers," *IEEE Access*, vol. 3, pp. 131–145, 2015.

[34] *"IEC 61000-4-21: EMC, Part 4: Testing and Measurement Techniques"*. Section 21: Reverberation Chamber Test Methods," Int. Electrotech.Comm., Geneva, Committee Draft, 2001.

[35] C. L. Holloway, D. A. Hill, J. M. Ladbury, P. F. Wilson, G. Koepke, and J. Coder, "On the use of reverberation chambers to simulate a rician radio environment for the testing of wireless devices," *IEEE Transactions on Antennas and Propagation*, vol. 54, no. 11, pp. 3167–3177, Nov 2006.

[36] J. M. Ladbury and D. A. Hill, "An improved model for antennas in reverberation chambers," in *2010 IEEE International Symposium on Electromagnetic Compatibility*, July 2010, pp. 663–667.

[37] J. Ladbury and D. A. Hill, "Enhanced backscatter in a reverberation chamber: Inside every complex problem is a simple solution struggling to get out," in *2007 IEEE International Symposium on Electromagnetic Compatibility*, July 2007, pp. 1–5.

[38] C. R. Dunlap, C. L. Holloway, R. Pirkl, J. Ladbury, E. F. Kuester, D. A. Hill, and S. van de Beek, "Characterizing reverberation chambers by measurements of the enhanced backscatter coefficient," in *2012 IEEE International Symposium on Electromagnetic Compatibility*, Aug 2012, pp. 210–215.

[39] K. A. Remley, R. J. Pirkl, H. A. Shah, and C. Wang, "Uncertainty from choice of mode-stirring technique in reverberation-chamber measurements," *IEEE Transactions on Electromagnetic Compatibility*, vol. 55, no. 6, pp. 1022–1030, Dec 2013.

[40] R. Vogt-Ardatjew, S. van de Beek, and F. Leferink, "Wide-band antennas for reverberation chambers," in *International Symposium on Electromagnetic Compatibility - EMC EUROPE*, Sept 2012, pp. 1–5.

[41] D. Mandaris and F. Leferink, "Simulation and measurement of log-periodic antenna and double ridged guide horn antenna for optimised field uniformity," in *2017 International Symposium on Electromagnetic Compatibility - EMC EUROPE*, Sept 2017, pp. 1–6.

[42] G. B. Tait and M. B. Slocum, "Random-walk technique for measuring the electromagnetic environment in electrically large reflective spaces," *IEEE Transactions on Instrumentation and Measurement*, vol. 60, no. 3, pp. 1003–1009, March 2011.

[43] *"LSProbe 1.2 Manual"*. Lumiloop GmbH. [Online]. Available: http://www.lumiloop.de/images/pdf/LSProbe_1v2_Users_Manual.pdf

[44] J. C. West, V. Rajamani, and C. F. Bunting, "Frequency- and time-domain measurement of reverberation chamber Q: An in-silico analysis," in *2016 IEEE International Symposium on Electromagnetic Compatibility (EMC)*, 2016, pp. 7–12.

[45] S. van de Beek, K. A. Remley, C. L. Holloway, J. M. Ladbury, and F. Leferink, "Characterizing large-form-factor devices in a reverberation chamber," in *2013 International Symposium on Electromagnetic Compatibility*, Sept 2013, pp. 375–380.

[46] B. N. Taylor and C. E. Kuyatt, "Guidelines for evaluating and expressing the uncertainty of NIST measurement results," NIST Tecnical Note 1297, Tech. Rep., 1994.

[47] K. Rosengren, P. Kildal, C. Carlsson, and J. Carlsson, "Characterization of antennas for mobile and wireless terminals by using reverberation chambers: improved accuracy by platform stirring," in *IEEE Antennas and Propagation Society International Symposium. 2001 Digest. Held in conjunction with: USNC/URSI National Radio Science Meeting (Cat. No.01CH37229)*, vol. 3, July 2001, pp. 350–353 vol.3.

Appendix A

Matlab script

This appendix shows the Matlab script that was used to obtain Q_{TD} from PDP. This Q_{TD} applies the method developed by Cristopher L. Holloway in the paper titled "Early Time Behaviour in Reverberation Chambers and Its Effect on the Relationships Between Coherence Bandwidth, Chamber Decay Time, RMS Delay Spread, and the Chamber Build-up Time" IEEE Trans. on EMC, August 2012.

```
%   FileData = string with the filename .mat obtained from the VNA
%   Frec = Array with frequencies of interest(GHz)
%   BW = Bandwidth (GHz)
%   N_pos = number of samples
%   PDP_dB = Power Delay Profile matrix
%   Q_TD = Time Domain Quality Factor
%   dBfall = number of dB for analyzing the PDP_dB fall time (for example 8 or 10 dB)
%   filter = moving average filter (for example 5)
%   Time = Time vector (s)
%   Trace = Amplitude vector (dB)

% ht_S21.m

function [ t, h_t ] = ht_S21(Fichero_Pos )

Freq=1e9.*Fichero_Pos(:,1);

L=length(Freq);

S11_Com=complex(Fichero_Pos(:,2),Fichero_Pos(:,3));

h_t=ifft(S21_Com);

Time_Res=1/(Freq(end)-Freq(1));

T_stop=Time_Res*(L-1);

t=0:Time_Res:T_stop;

end

% PostprocessPDP_QTD2.m
```

```
33
34 function [ PDP_dB, Q_TD] = PostprocessPDP_QTD2( ...
       FileData,Frec,BW,N_pos,dB_fall,filter  )
35
36 close all
37
38 load(FileData);
39 % Vars Inizilization
40 PDP_dB=zeros(max(size(Pos_1)),length(Frec))-99;
41 Q_TD=zeros(length(Frec),1);
42
43 for index=1:length(Frec)
44     % Selected bandwidth
45     j=find(Pos_1(:,1)>Frec(index)-BW/2);
46     k=find(Pos_1(:,1)>Frec(index)+BW/2);
47     if isempty(k)
48         k=max(size(Pos_1));
49     end
50
51     ht=zeros(k(1)-j(1)+1,N_pos);
52     % Impulse response function
53     for i=1:N_pos
54         orden=['[t ht(:,' int2str(i) ')]=ht_S21(Pos_' int2str(i) '(' int2str(j(1)) ...
               ':' int2str(k(1)) ',:));'];
55         eval (orden);
56     end
57
58     ht_abs_mean=mean(abs(ht).^2,2);
59
60     Max_ht=max(ht_abs_mean);
61     % Normalization and natual log application
62     PDP_dB(1:length(t),index)=log(ht_abs_mean./Max_ht);
63
64     % Finding the slope
65     Index_t=find(smooth(PDP_dB(:,index),filter)>-1*dB_fall);
66
67     % Restart the Index
68     kk=1;
69     Aux=zeros(1,length(Index_t));
70     Aux(kk)=Index_t(kk+1)-Index_t(kk);
71     while (Aux(kk)==1)&&(kk<length(Index_t)-1)
72           kk=kk+1;
73           Aux(kk)=Index_t(kk+1)-Index_t(kk);
74     end
75     Index_t=Index_t(1:kk);
76
77     % Comment or uncomment the figure plot if you want to check the PDP(t)
78     % Smoothing filter application
79     figure;plot(t(Index_t),smooth(PDP_dB(Index_t,index),filter));
80     % Quality factor calculation function
81     [ Q_TD(index) ] = Q_TD_Holloway_LinearFit( t(Index_t), ...
           smooth(PDP_dB(Index_t,index),filter) , Frec(index)*1e9);
82
83 end
84
85 %Q_TD_Holloway_LinearFit.m
```

```
86
87  function [ Q_TD ] = Q_TD_Holloway_LinearFit( Time, Trace , Frec)
88
89  Ut=find(Trace==max(Trace));
90
91  Lt=find(Trace==min(Trace));
92
93  if Lt<Ut
94      Lt=length(Trace);
95  end
96
97  Slope=Ut:Lt;
98
99  fitResults1 = polyfit(Time(Slope)',Trace(Slope), 1);
100
101 % Comment or uncomment the figure plot if you want to check the PDP(t)
102 figure;plot(Time(Slope),Trace(Slope));
103
104 Q_TD=(2*pi()*Frec)*(-1/fitResults1(1));
105
106 end
```